



Computer-aided working-fluid design, thermodynamic optimisation and thermoeconomic assessment of ORC systems for waste-heat recovery

M.T. White ^{a, b}, O.A. Oyewunmi ^a, M.A. Chatzopoulou ^a, A.M. Pantaleo ^{a, c}, A.J. Haslam ^a, C.N. Markides ^{a, *}

^a Clean Energy Processes (CEP) Laboratory, Department of Chemical Engineering, Imperial College London, South Kensington Campus, London SW7 2AZ, UK

^b Department of Mechanical Engineering and Aeronautics, City, University of London, Northampton Square, London EC1V 0HB, UK

^c Department of Agro-environmental Sciences, University of Bari, Via Amendola 165/A, 70125, Bari, Italy

ARTICLE INFO

Article history:

Received 29 December 2017

Received in revised form

13 June 2018

Accepted 15 July 2018

Available online 19 July 2018

Keywords:

Organic Rankine cycle

ORC

Computer-aided molecular-design

CAMD

Group contribution

SAFT- γ Mie

Thermoeconomic

ABSTRACT

The wider adoption of organic Rankine cycle (ORC) technology for power generation or cogeneration from renewable or recovered waste-heat in many applications can be facilitated by improved thermodynamic performance, but also reduced investment costs. In this context, it is suggested that the further development of ORC power systems should be guided by combined thermoeconomic assessments that can capture directly the trade-offs between performance and cost with the aim of proposing solutions with high resource-use efficiency and, importantly, improved economic viability. This paper couples, for the first time, the computer-aided molecular design (CAMD) of the ORC working-fluid based on the statistical associating fluid theory (SAFT)- γ Mie equation of state with thermodynamic modelling and optimisation, in addition to heat-exchanger sizing models, component cost correlations and thermoeconomic assessments. The resulting CAMD-ORC framework presents a novel and powerful approach with extended capabilities that allows the thermodynamic optimisation of the ORC system and working fluid to be performed in a single step, thus removing subjective and pre-emptive screening criteria that exist in conventional approaches, while also extending to include cost considerations relating to the resulting optimal systems. Following validation, the proposed framework is used to identify optimal cycles and working fluids over a wide range of conditions characterised by three different heat-source cases with temperatures of 150 °C, 250 °C and 350 °C, corresponding to small- to medium-scale applications. In each case, the optimal combination of ORC system design and working fluid is identified, and the corresponding capital costs are evaluated. It is found that fluids with low specific-investment costs (SIC) are different to those that maximise the power output. The fluids with the lowest SIC are isoheptane, 2-pentene and 2-heptene, with SICs of £5620, £2760 and £2070 per kW respectively, and corresponding power outputs of 32.9 kW, 136.6 kW and 213.9 kW.

© 2018 The Authors. Published by Elsevier Ltd. This is an open access article under the CC BY license (<http://creativecommons.org/licenses/by/4.0/>).

1. Introduction

Despite the growing interest in the utilisation of renewable and sustainable thermal-energy sources, as well as in improving energy efficiency and reducing fossil-fuel consumption and our impact on the environment, there remains a lack of widespread deployment of relevant technologies and a significant amount of waste heat that is currently rejected to the atmosphere. Of the many technologies

that can be considered for the conversion of renewable or recovered waste-heat into electricity, including some recently proposed novel two-phase cycles such as the non-inertive-feedback thermofluidic engine (NIFTE) [1–5] and Up-THERM heat converter [6–9], the organic Rankine cycle (ORC) [10–13] is one of the most promising and mature candidates, and is suitable for low- and medium-grade heat sources, typically at temperatures between 80 and 400 °C [14,15].

One of the most important elements of an ORC system is the working fluid that undertakes the thermodynamic cycle. As such, the selected fluid affects system performance and operation, as well

* Corresponding author.

E-mail address: c.markides@imperial.ac.uk (C.N. Markides).

as component design, size and cost. With increasingly more stringent legislation, fluids such as chlorofluorocarbons (CFCs) have already been phased out, whilst fluids such as hydrochlorofluorocarbons (HCFCs) and hydrofluorocarbons (HFCs) are set to be phased out in the coming years [16]. From the perspective of an end-user, technical solutions are required that are both environmentally friendly and economically feasible. This demands the identification of both novel fluids that meet all legislative requirements, and ORC systems that are optimised in terms of economic performance indicators such as the net-present value (NPV) or the levelised cost of energy (LCOE).

During a conventional working-fluid selection study an optimal working fluid is typically selected after screening a group of fluids based on predefined criteria and then conducting a parametric optimisation study [17,18]. However, such an approach cannot be used to identify new and potentially novel working fluids, and therefore more holistic approaches are required. For example, Drescher and Brüggemann [19] identified five optimal working fluids for a biomass application from an initial group of 1800 substances, whilst Schwöbel *et al.* [20] devised a working-fluid screening process and applied it to 3174 potential working fluids. More recently, Preißinger *et al.* [21] combined computational chemistry techniques with a thermodynamic process simulation, and applied a multi-criteria evaluation technique to 72 million chemical substances. Other authors have attempted a more generalised approach to working-fluid selection, by developing correlations that relate working-fluid parameters, such as the critical temperature, to the heat source conditions [22,23].

Alternatively, computer-aided molecular design (CAMD) can be used to provide a more holistic approach to working-fluid selection. In CAMD, a potential working fluid is described by functional groups, which can be put together in different ways to form different molecules. For example, the $-\text{CH}_3$, $-\text{CH}_2-$, $>\text{C}-$, $>\text{C}<$, $=\text{CH}_2$, and $=\text{CH}-$ groups can be combined to generate a large number of hydrocarbon working fluids. Then, if an equation of state is available that can predict thermodynamic properties based on the functional groups from which it is composed, the molecular structure of the working fluid can be simultaneously optimised alongside the ORC system. In this sense, CAMD-ORC models have the potential to identify novel working-fluids which may otherwise be overlooked, whilst removing pre-emptive and subjective screening criteria.

Papadopoulos *et al.* [24] used CAMD to identify potential working-fluid candidates before completing a more conventional ORC process simulation, and later applied CAMD to the optimal design of working-fluid mixtures [25]. Brignoli and Brown [26] used group-contribution methods to investigate the effect of a working-fluid's critical point on the thermodynamic performance of the ORC, whilst Palma-Flores *et al.* [27] demonstrated the potential of CAMD to identify new fluids with higher thermal efficiencies and better safety characteristics. Furthermore, Su and Deng [28] developed a thermodynamic ORC model, and later implemented this into a CAMD-ORC framework [29]. Cignitti *et al.* [30] also developed a CAMD-ORC model and, in addition to optimising thermodynamic performance, considered the associated heat-exchanger requirements. Nevertheless, these previous studies have relied on empirical group-contribution methods, such as the Joback and Reid method [31], to obtain working-fluid parameters including the critical temperature and pressure from which thermodynamic properties can be calculated using a cubic equation of state. More advanced group-contribution equations of state have also been applied within a CAMD-ORC framework, which use molecular-based equations of state based on statistical associating fluid theory (SAFT) [32,33]. Lampe *et al.* [34,35] developed a CAMD-

ORC model based on the PC-SAFT equation of state [36,37], and used this model to optimise ORC systems for a geothermal application. The CAMD-ORC optimisation was split into two stages. In the first stage an optimal, but hypothetical, working fluid was identified, and in the second stage real working fluids with similar performance were identified. Later, Schilling *et al.* [38] reduced the problem to a single stage optimisation in which the working-fluid structure and ORC system are simultaneously optimised, and has recently extended the model to include transport properties and cost correlations, facilitating the specific-investment cost to be determined [39].

With a few exceptions, the major limitation of previous CAMD-ORC models has been a focus on optimising the cycle and its thermodynamic performance; nevertheless, achieving the successful commercialisation of ORC systems across a range of applications requires a consideration of thermoeconomic performance. Quoilin *et al.* [40] evaluated the specific-investment cost (SIC) of small-scale waste-heat driven ORC units, whilst Lecompte *et al.* [41] optimised the design of ORC units for large-scale CHP plants and waste-heat recovery. Multi-objective optimisation studies can be also found in the literature [42–44], where the authors considered the trade-off between maximising power output whilst minimising the SIC. However, all of these previous thermoeconomic studies consider only predefined working fluids, and conduct a separate optimisation for each specific fluid. On the contrary, thermoeconomic methods have not been previously applied to CAMD-ORC models, partly due to the requirement of group-contribution methods for determining transport properties to size the system heat exchangers.

Another limitation to previous CAMD-ORC models is that they have focussed typically only on non-recuperated and subcritical ORC systems. However, there exist opportunities to improve the thermodynamic performance of this basic ORC by changing the cycle architecture. For example, using a working-fluid mixture instead of a pure fluid results in non-isothermal, isobaric phase change processes, which facilitates a better thermal match between the working fluid and heat source, and between the working fluid and heat sink, thus reducing irreversibilities and improving the thermodynamic performance of the cycle [42,45,46]. Alternatively, operating a partially-evaporated cycle, in which expansion occurs from a two-phase state, can also be used to increase the power output from system [47,48].

The authors of the current paper have previously developed a CAMD-ORC framework, based on the SAFT- γ Mie group-contribution equation of state [49]. In this previous work, empirical group-contribution transport property prediction methods for hydrocarbon working fluids were validated against NIST REFPROP [50]. The aim of the current study is to combine these transport property prediction methods with a heat-exchanger sizing model and integrate this model into the CAMD-ORC framework. This, in turn, allows a thermoeconomic assessment of the system to be conducted following a thermodynamic optimisation, and therefore optimal working fluids to be identified based on thermoeconomic performance indicators. In addition, the current paper extends the thermodynamic model, such that recuperated, partially-evaporated and working-fluid mixture cycles can all be considered within the CAMD-ORC framework. It is noted that although models for these novel cycles are presented and validated in this paper, they are not considered further in the case studies since suitable methods for predicting the heat transfer in complex flows of fluid mixtures and cost correlations for two-phase expanders are not readily available. However, their inclusion is justified as it facilitates these novel systems to be evaluated in the future. As far as the authors are aware, this is the first study that details a complete

CAMD-ORC framework, based on an advanced group-contribution equation of state, that can conduct a thermoeconomic assessment in this manner, in addition to simulating novel cycle architectures.

In what follows, the key aspects the CAMD-ORC framework are discussed in Section 2, including the group-contribution methods, the thermodynamic model, and the component sizing and costing models, which are then validated in Section 3. The framework is applied to three case studies that consider the design of hydrocarbon working-fluids and corresponding optimised ORC systems in Section 4, and some further economic considerations are discussed in Section 5. Finally, the key findings from this study are summarised in Section 6.

2. CAMD-ORC model

2.1. Group-contribution methods

Group-contribution methods determine the properties of a particular molecule based on the functional groups that make it up. For example, isopentane is described by three $-\text{CH}_3$ groups, one $-\text{CH}_2-$ and one $>\text{CH}-$ group. In a group-contribution method group parameters are only required for the individual groups, which allows the evaluation of novel working fluids for which property prediction would not be possible using conventional approaches. To capture the trade-off between thermodynamic performance and system costs, group-contribution methods are required for both the thermodynamic properties and transport properties. In this work, the SAFT- γ Mie equation of state [51] is used for thermodynamic property prediction. SAFT- γ Mie is a state-of-the-art version of statistical associating fluid theory (SAFT) [32,33] wherein a Mie potential is used to model the interaction between two molecular groups [51]. Group parameters are available for the hydrocarbon groups considered within this paper, and have been validated against experimental data [52]. Unfortunately, SAFT- γ Mie is only suitable for determining thermodynamic

properties, so alternative methods are required to predict the dynamic viscosity μ , thermal conductivity k and surface tension σ . Previously, empirical group-contribution methods for the prediction of these properties have been applied to hydrocarbon working fluids, and validated against data from NIST [49]. The correlations applied here are summarised in Table 1, and are reviewed in detail in Ref. [49].

2.2. Thermodynamic modelling

The thermodynamic analysis of the ORC is well described within the literature, and consists of applying an energy balance to each component within the cycle. Besides analysing basic, non-recuperated and subcritical cycles, the CAMD-ORC model has also been extended to be suitable for the evaluation of cycles operating with mixtures, recuperated cycles, and cycles with partial evaporation. A schematic representation of each cycle architecture, and the prescribed notation is given in Fig. 1.

For all cycles, the system is assumed to be in a steady state, pressure drops within the heat exchangers and piping are neglected, whilst the condensation temperature T_1 and reduced pressure p_r (p_2/p_{cr} , where p_2 and p_{cr} are the evaporation and critical pressures respectively) are both defined as optimisation variables. Moreover, values for the pump isentropic efficiency η_p and expander isentropic efficiency η_e are fixed. In this paper, the expander is assumed to be a radial turbine for which extensive information can be found in the literature, and which is suitable for the power ranges being considered while being capable of achieving large expansion ratios across a single stage. It is acknowledged that the assumption of a single fixed turbine isentropic efficiency over a range of system sizes operating with different expansion ratios is an oversimplification. However, these effects have been neglected owing to the complexity of requiring a more detailed expander model, which is not a particular focus of this work, but could be included in the future.

Table 1
Summary of group-contribution methods used within the CAMD-ORC framework.

Property	Liquid phase	Vapour phase
Thermodynamic (T, p, h, s, ρ)		SAFT- γ Mie [51]
Critical (T_{cr}, p_{cr}, V_{cr})		Joback-Reid [31]
Surface tension (σ)		Sastri-Rao [53]
Dynamic viscosity (μ)	Joback-Reid [31] (n-alkanes) Sastri-Rao [56] (branched alkanes)	Reichenberg [54,55]
Thermal conductivity (k)	Sastri [57]	Chung [58,59]

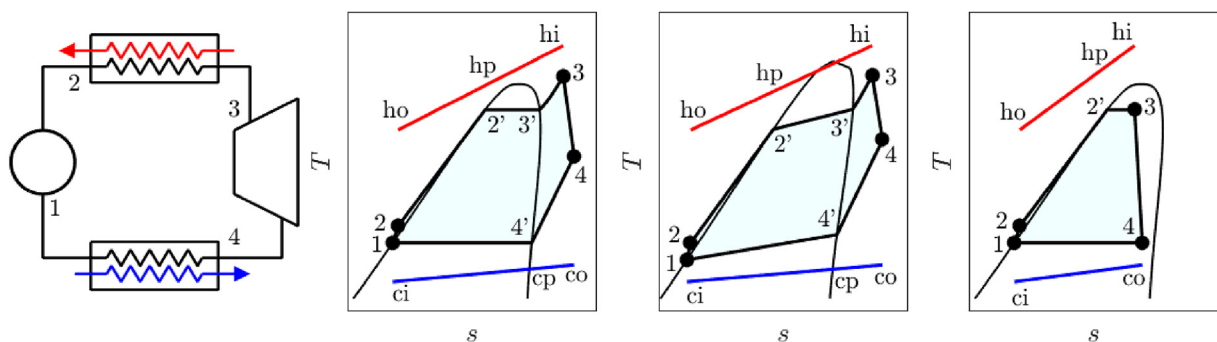


Fig. 1. Schematic of the ORC system and the different cycle architectures represented on a T-s diagram. From left to right: cycle schematic, basic non-recuperated, mixture and partially-evaporated.

Alongside T_1 and p_r an additional optimisation variable is required to define all the state points within the cycle, and this is defined using the notation z . This parameter is introduced to allow both superheated and partially-evaporated cycles to be modelled using one optimisation variable, which varies between 0 and 2. When $0 \leq z \leq 1$, two-phase expansion is assumed and z is equal to the expander inlet vapour quality. When $1 < z \leq 2$, the working fluid expands from a superheated state and the amount of superheating ΔT_{sh} is given by:

$$\Delta T_{sh} = (z - 1)(T_{hi} - T_{3'}), \quad (1)$$

where T_{hi} is the heat-source inlet temperature and $T_{3'}$ is the saturated-vapour temperature. It is noted that when $z = 2$, $T_{hi} = T_3$ which would imply an infinitely large heat exchanger. Therefore, within an optimisation a minimum evaporator pinch constraint is imposed ($T_{hi} - T_{3'} > PP_{h,min}$), which will always result in cycles where $z < 2$.

The working-fluid mass flow rate \dot{m}_o (kg/s) is determined by imposing the evaporator pinch point PP_h at the start of evaporation (i.e., $PP_h = T_{hp} - T_{2'}$), and applying an energy balance:

$$\dot{m}_o = \frac{(\dot{m}c_p)_h (T_{hi} - T_{hp})}{h_3 - h_{2'}}, \quad (2)$$

where $(\dot{m}c_p)_h$ is the heat-capacity rate of the heat source (W/K) and $h_{2'}$ and h_3 are the enthalpies (J/kg) of the working fluid at the start of evaporation and expander inlet respectively. With the mass-flow rate known, the thermodynamic performance of the ORC can be evaluated by determining the net power output from the system \dot{W}_n (W):

$$\dot{W}_n = \dot{m}_o[(h_3 - h_4) - (h_2 - h_1)] \quad (3)$$

Finally, an energy balance is applied to the condenser to obtain the condenser pinch point PP_c . This is given by:

$$PP_c = T_4 - \frac{\dot{m}_o(h_4 - h_1)}{(\dot{m}c_p)_c}, \quad (4)$$

if the expansion process ends in two-phase region, and:

$$PP_c = T_{4'} - \frac{\dot{m}_o(h_{4'} - h_1)}{(\dot{m}c_p)_c}, \quad (5)$$

if the expansion process ends in the superheated region. Within the model, the minimum allowable condenser pinch point $PP_{c,min}$ is defined as a constraint.

The calculation process described so far is applicable to all types of cycle, but for working-fluid mixtures and recuperated cycles, additional parameters are introduced. For a mixture both working fluids are described by their functional groups and the variable x is introduced to represent the mass fraction of the first fluid. A recuperated cycle is modelled by a fixed recuperator effectiveness ϵ_r , and the inclusion of a recuperator is defined by a binary flag.

2.3. Component sizing

The evaporator and condenser are assumed to be tube-in-tube heat exchangers, which are cost effective for small- to medium-scale applications [60]. The heat exchangers are sized by determining the total required heat-transfer area, which is obtained by calculating the heat-transfer coefficient in the different single- and two-phase heat-transfer regions. In the evaporator this corresponds to single-phase preheating, two-phase evaporation and

single-phase superheating regions, and in the condenser it corresponds to single-phase desuperheating and two-phase condensation regions.

Depending on the heat-transfer region, different Nusselt-number correlations are applied to determine the local heat-transfer coefficient. For single-phase heat transfer the Dittus-Boelter [61] correlation has been used. For evaporation, the correlations proposed by Cooper [60] and Gorenflo [62] have been used for nucleate-boiling conditions, whereas the Dobson [63] and Zuber [60] correlations have been used to account for the convective-heat-transfer phenomena. For condensation inside tubes, the correlations proposed by Shah [64] and Dobson [63] have been considered, accounting for both gravity-driven and shear-driven condensation. The reader can refer to Ref. [65] for a detailed analysis and comparison of the correlations selected. The Nusselt-number correlations for two-phase heat transfer are typically a function of the vapour quality, which varies along the length of the heat exchanger. Therefore, the heat-exchanger length is discretised into n segments of equal heat duty. For each segment the vapour quality is assumed to be constant and an estimate for the heat-transfer area for that segment is obtained.

Expressed mathematically, the total heat-transfer area for a given heat exchanger A (m²) is given as the summation of all the segments:

$$A = \sum_{i=1}^n \frac{\dot{Q}_i}{U_i \Delta T_{log,i}}, \quad (6)$$

where \dot{Q}_i and $\Delta T_{log,i}$ are the heat-transfer rate (W) and counter-flow log-mean temperature difference (K) for segment i respectively, and U_i is the overall heat-transfer coefficient (W/(m² K)) for segment i and is found based on the heat-transfer coefficients on either side of the heat-exchanger wall.

A key consideration when estimating the required heat-transfer area is the pressure drop along the full length of the heat exchanger. In this study, a number of pressure drop correlations have been used to predict the pressure drop of the organic working fluid, the heat source fluid (Therminol 66) and the cooling fluid (water) inside the heat exchangers. For both the evaporator and the condenser units the pressure drop was restricted to not exceed 1 – 2 bar, which is in line with good-practice industry standards. For the single-phase zone, the pressure drop is calculated as a function of the fluid velocity inside the tubes, the diameter of tubes, the length of the heat exchanger, and a friction coefficient. The calculation is completed using the following set of equations in line with [60]:

$$Re = \rho u D / \mu; \quad (7)$$

$$f = 0.046 Re^{-0.2}; \quad (8)$$

$$\Delta P = 4f \frac{L}{D} \frac{\rho u^2}{2}, \quad (9)$$

where Re is the Reynolds number, ρ is the fluid density (kg/m³), u is the fluid velocity (m/s), D is the tube diameter (characteristic length) (m), μ is the dynamic viscosity (Pa s), f is a friction factor (also referred to as the Fanning friction factor), L is the heat exchanger length (m), and ΔP is the pressure drop (Pa). For the two-phase zone pressure drop, the correlation developed by Chisholm as presented in Ref. [60] has been used. The equations for the two phase zone pressure drop have been omitted here for brevity.

2.4. Thermoeconomic analysis

Since there are only a limited number of ORC applications worldwide, and system cost data are not publicly available, cost correlations originating from the chemical industry are commonly used in the literature. A well-established method is the module costing technique [66], which provides the costs of individual components, based on a specific sizing attribute (e.g., heat-transfer area for heat exchangers, etc.). By adding the individual component costs the total ORC unit cost is obtained. The costing method applied within this study is summarised in Refs. [65,67] and uses the cost correlations given by Seider *et al.* [68]:

$$C_p^0 = F \exp(Z_1 + Z_2 \ln(X) + Z_3 \ln(X)^2 + Z_4 \ln(X)^3 + Z_5 \ln(X)^4), \quad (10)$$

and Turton *et al.* [69]:

$$C_p^0 = F10^{(Z_1 + Z_2 \log(X) + Z_3 \log(X)^2)}, \quad (11)$$

where C_p^0 is the component cost in £; F is a material factor accounting for the component manufacturing; Z_i is the cost coefficient; and X is the sizing attribute. Both Z_i and X vary depend on the type of the equipment selected and the values used to estimate the purchase cost of each piece of equipment are summarised in Table 2. It is assumed that the pump is a centrifugal pump, whilst the heat exchangers are of a tube-in-tube construction. As previously stated, the expander is assumed to be a radial turbine, and this component's cost is based only on the power output. In reality, the expansion ratio of the turbine will impact both the expander efficiency and cost. Within this work these effects have been neglected owing to the complexities of requiring a more detailed expander model, and because correlations that consider these effects are either not currently available, or not sufficiently validated. However, these effects should be considered in future studies. Finally, the Chemical Engineering Plant Cost Index (CEPCI) is used to convert the cost to today's values. For Turton *et al.* [69] the basis year is 2001 (CEPCI₂₀₀₁ = 397), whilst for Seider *et al.* [68] the basis year is 2006 (CEPCI₂₀₀₆ = 500). The costs are converted to today's values using CEPCI₂₀₁₇ = 562.1.

2.5. Optimisation

The CAMD-ORC framework is formulated in gPROMS [70], and the optimisation is completed using the OAERAP outer-approximation algorithm. The optimisation concerns integer variables describing the working-fluid molecular structure and continuous variables describing the power system, and therefore is a mixed-integer non-linear programming (MINLP) problem. The optimisation is solved by first relaxing the integer variables to continuous variables and completing a non-linear programming (NLP) optimisation, which in turn supplies a maximum for the objective function. The MINLP is then solved by successive iterations of a mixed-integer linear programming problem (MILP), in

which the objective function and constraints are linearised, and an additional NLP in which the power system variables are optimised for a particular fluid identified from the MILP. The general optimisation is formulated as:

$$\max f(\mathbf{x}, \mathbf{y}), \quad (12)$$

subject to:

$$\mathbf{x}_{\min} \leq \mathbf{x} \leq \mathbf{x}_{\max}; \quad (13)$$

$$\mathbf{y}_{\min} \leq \mathbf{y} \leq \mathbf{y}_{\max}; \quad (14)$$

$$g(\mathbf{x}, \mathbf{y}) \leq 0; \quad (15)$$

$$h(\mathbf{x}, \mathbf{y}) \leq 0; \quad (16)$$

where $f(\mathbf{x}, \mathbf{y})$ is the objective function to be maximised, \mathbf{x} and \mathbf{y} are vectors containing system and working-fluid variables respectively, the inequalities in Eqs. (13) and (14) represent the lower and upper bounds for the variables, and $g(\mathbf{x}, \mathbf{y})$ and $h(\mathbf{x}, \mathbf{y})$ are the cycle and molecular constraints respectively.

In this work, the objective of the optimisation is to maximise the ORC system power output W_n , which is followed by economic assessments of the optimal systems. However, future research should integrate the economic analysis into the optimisation model and include direct considerations of thermoeconomic performance indicators such as the specific-investment cost. It is intended that such optimisation exercises will be performed in the future using further extensions of the existing CAMD-ORC framework.

3. Model validation

3.1. Thermodynamic and transport property validation

Within the CAMD-ORC framework group-contribution methods are used to predict both the thermodynamic and transport properties of the working fluid. As discussed previously, SAFT- γ Mie is used to predict the thermodynamic properties, and a number of different empirical correlations are used for the transport properties. The non-group-contribution formulation of SAFT- γ Mie, SAFT-VR Mie [71,72], has previously been applied to the study of optimal working-fluid mixtures for ORC systems, in which the average absolute deviation in saturation properties (density and pressure), specific-heat capacities and critical properties (temperature and pressure), in comparison to the values provided by NIST REFPROP, are all below 5% for the pure alkane and perfluoroalkane fluids considered [73]. Furthermore, SAFT- γ Mie has also been shown to provide an accurate description of fluid-phase thermodynamic properties for a wider variety of fluids [50–52,74]. Moreover, the authors of the current paper have also validated SAFT- γ Mie within the context of the existing CAMD-ORC framework [49], which also involved the validation of the group-contribution transport

Table 2
Cost correlations coefficients.

Component	Attribute (X)	F	Z_1	Z_2	Z_3	Z_4	Z_5	Ref.
Expander	Power, W_e (kW)	3.5	2.2486	1.4965	−0.1618	0	0	[69]
Pump	S^a	2.7	9.2951	−0.6019	0.0519	0	0	[68]
Pump motor	Power, W_p (HP)	1.4	5.83	0.134	0.0533	0.0286	0.00355	[68]
Evaporator - Condenser	Area (m^2)	1	9.5638	0.532	−0.0002	0	0	[68]
Preheater - Desuperheater	Area (m^2)	1	10.106	−0.4429	0.0901	0	0	[68]

^a $S = \dot{V}\sqrt{H}$ where \dot{V} is the pump volumetric flow rate in gallons per minute and H is the pump head in feet.

property prediction methods. It was found that the absolute deviations of the critical temperatures and pressures of the selected hydrocarbon working fluids were less than 0.5% and 4% respectively. The average absolute deviations of the viscosity, thermal conductivity and surface tension with respect to available experimental data, evaluated at temperatures between 20 °C and 400 °C, were generally less than 4%, 5% and 8% respectively. Overall, this provides reasonable confidence in the suitability of the group-contribution methods employed within this current work.

3.2. Cycle modelling

In our previous work, the CAMD-ORC model has been validated for a non-recuperated, subcritical ORC operating with an array of hydrocarbon working fluids, by comparing the results to a similar model that uses the NIST REFPROP program to calculate thermodynamic properties [49]. Both models were found to identify optimal cycles with very similar reduced evaporating pressures, whilst the maximum power output predicted by the CAMD-ORC model deviated by less than 1.5% compared to the REFPROP model.

In this section, a similar validation study is completed to confirm the suitability of the CAMD-ORC model to simulate the alternative cycle architectures introduced in Section 2.2, namely cycles operating with working-fluid mixtures and partially-evaporated cycles. Although the model is expected to be applicable for the range of heat-source temperatures relevant to ORC systems (*i.e.*, 373–673 K), the heat source is assumed to be at 473 K for the validation study. It is easily shown that the thermodynamic performance of an ORC system is independent of the heat-source mass-flow rate and therefore the heat source is defined with a heat-capacity rate of $\dot{m}c_p = 4.2 \text{ kW/K}$. Finally, the pump and expander are modelled by assuming fixed isentropic efficiencies of $\eta_p = 0.7$ and $\eta_e = 0.8$ respectively, whilst $T_1 = 303 \text{ K}$ and $PP_{h,\min} = 10 \text{ K}$ are assumed; these values are considered to be representative of a typical ORC system.

3.2.1. Partially-evaporated cycles

The purpose of the first validation study is to confirm the suitability of the CAMD-ORC model for partially-evaporated cycles. Five different working fluids were considered for this study, namely *n*-pentane, *n*-hexane, *n*-heptane, isopentane and isohexane, and a parametric study was performed in which z was varied between 0 and 2, which was repeated at different evaporation pressures. A comparison between the results obtained using the CAMD-ORC model, based on SAFT- γ Mie, and a similar model using NIST REFPROP is given in Fig. 2. In this figure, the results for only three fluids are shown, however the other two fluids were found to follow the same behaviour. The 18.6 and 24.9 bar cases for *n*-hexane do not appear in Fig. 2 because the saturation temperature of *n*-hexane at these pressures is higher than the heat-source temperature.

Overall, it is observed that, except for the 28.0 bar cases for *n*-pentane and isopentane, a very good agreement between the two models is obtained. Neglecting these two cases, the maximum deviations between the CAMD-ORC model and REFPROP model are below 4%, 1% and 5% for *n*-pentane, *n*-hexane and isopentane respectively. For *n*-heptane and isohexane, the maximum deviations are below 2% and 3% respectively. Ultimately, this validates the suitability of the CAMD-ORC model to simulate these types of cycles. The deviation for the 28.0 bar isopentane case can be explained because at higher pressures the cycle is operating closer to the critical point (33.8 bar), and the deviation between SAFT- γ Mie and NIST REFPROP is found to increase as the critical point is approached.

More generally, from Fig. 2 it is observed that the maximum

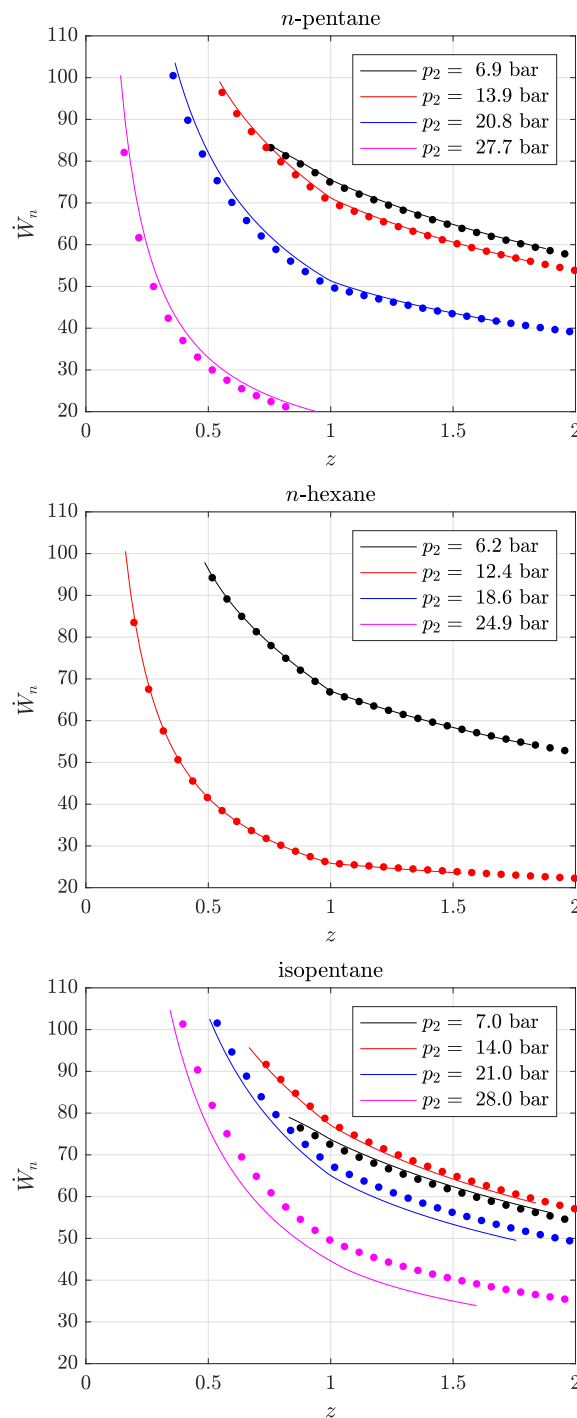


Fig. 2. Comparison between the power output (\dot{W}_n in kW) predicted by the CAMD-ORC model (circular markers) and predicted by a model using NIST REFPROP for thermodynamic properties (continuous curves) for three different working fluids operating within a partially-evaporated ($z < 1$) and a superheated ($z \geq 1$) cycle.

power is always generated when $z < 1$. This is due to the fact that expansion when $z < 1$ takes place inside the two-phase region, such that a larger proportion of the heat transfer during heat addition occurs during preheating, and results in a lower heat-source outlet temperature, T_{ho} . This, in turn, means that the ORC is capable of extracting more heat from the heat source, leading to a higher power output. This clearly indicates the potential thermodynamic performance benefit of allowing the working fluid to expand from a

two-phase state.

3.2.2. Working-fluid mixtures

For the validation of the CAMD-ORC model for mixtures, three different mixtures were considered, namely *n*-hexane/*n*-butane, *n*-heptane/*n*-butane and *n*-heptane/*n*-pentane. For each mixture a parametric study was completed in which the mass fraction of Fluid 1, x , was varied from 0 to 1, and this was repeated at different

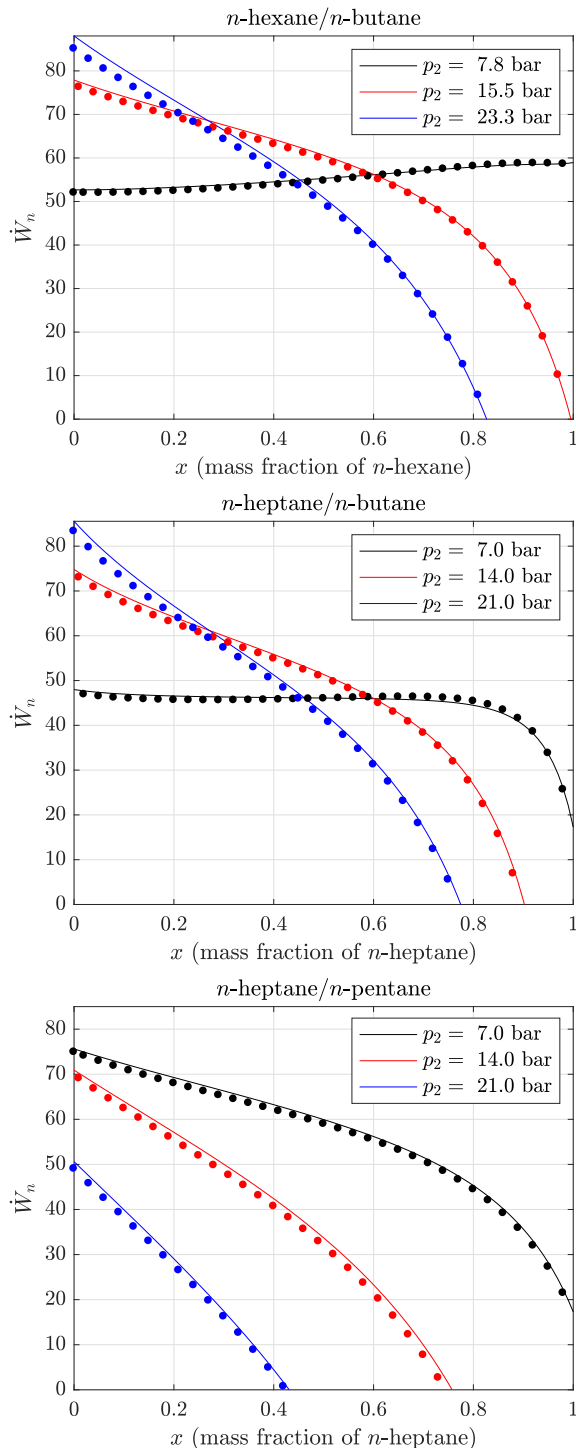


Fig. 3. Comparison between the power output (\dot{W}_n in kW) predicted by the CAMD-ORC model (circular markers) and predicted by a model using NIST REFPROP for thermodynamic properties (continuous curves) for three different fluid mixtures.

evaporation pressures. In each case, it was assumed that expansion occurs from a saturated-vapour state (i.e., $z = 1$). A comparison between the results obtained using the CAMD-ORC model and the model based on NIST REFPROP is shown in Fig. 3. Again, a very good agreement is observed for the different case studies; neglecting power outputs below 20 kW, which do not represent good thermodynamic cycles, the maximum deviations between the CAMD-ORC and REFPROP models are 4%, 4% and 8% for the *n*-hexane/*n*-butane, *n*-heptane/*n*-butane and *n*-heptane/*n*-pentane cases respectively. These results, therefore, validate the CAMD-ORC model for simulating these types of cycles.

3.3. Heat-exchanger sizing validation

The CAMD-ORC framework has been used previously to optimise the working fluid and cycle conditions for non-recuperated subcritical ORCs for three different waste-heat streams [49]. Now, using the group-contribution transport-property prediction methods and the heat-exchanger sizing model described in Sections 2.1 and 2.3, it is possible to determine the area requirements of the evaporator and the condenser for these optimum cycles. The full analysis will be described in detail in Section 4, however, first, it is necessary to validate the developed extended model.

For this validation study, heat-exchanger sizing is first performed using properties obtained from NIST REFPROP, after which the results are compared to those obtained using the group-contribution transport properties. Not all of the fluids considered in the initial CAMD-ORC optimisation study are available within REFPROP, and therefore it is only possible to validate the model for a subset of the fluids considered. This subset of fluids used for the comparison study includes *n*-propane (*n*-alkane), isobutane (methyl alkanes), 1-propene (1-alkene) and cis-2-butene (2-alkene). The heat-carrier fluid for all fluids is Therminol 66, entering the evaporator at 150 °C and 1 bar.

The evaporator and condenser area requirements for the four working fluids are presented in Figs. 4 and 5. The results obtained using the group-contribution transport property model are in good agreement with those obtained from REFPROP. The heat-exchanger area calculations for *n*-propane and isobutane have negligible difference between the two methods. The highest deviation is recorded for cis-2-butene, where the condenser unit surface area is overestimated by the group-contribution method by approximately 18%, being on the conservative side of the heat-exchanger design. It should be noted that the Nusselt number correlations

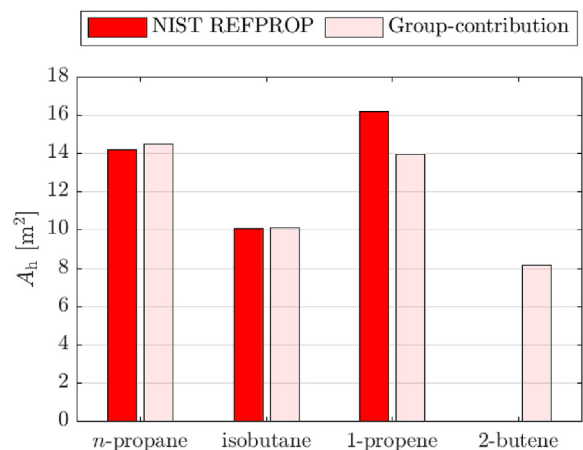


Fig. 4. Comparison between the evaporator area (A_h in m²) obtained using group-contribution transport properties and NIST REFPROP.

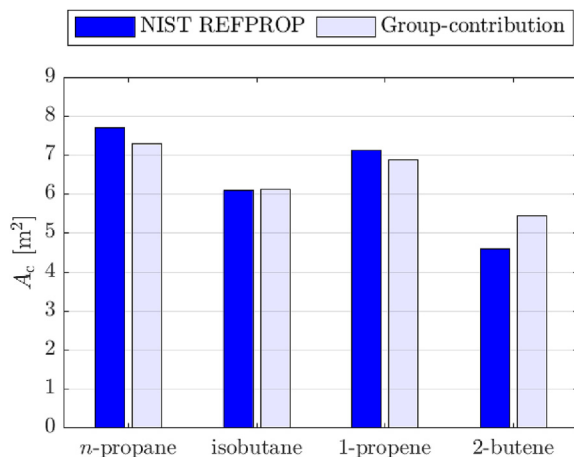


Fig. 5. Comparison between the condenser area (A_c in m^2) obtained using group-contribution transport properties and NIST REFPROP.

for the evaporator area calculation require the use of the working fluid surface tension, which for *cis*-2-butene is not available in NIST.

Compared to the *n*-propane and isobutane cases, the 1-propene case shows a relatively large deviation of 13.9% between the total evaporator area predicted using the CAMD-ORC model and REFPROP. This deviation occurs, in part, because it is not possible to match exactly the thermodynamic cycle conditions input into the heat-exchanger sizing model, and those output from the CAMD-ORC model. This, coupled with the higher superheating degree of the 1-propene cycle, which is 54 °C compared to 18 °C and 0.1 °C for the *n*-propane and isobutane cycles, results in the 1-propene superheater load for the REFPROP heat-exchanger sizing model being higher than the CAMD-ORC model. Considering that the heat-transfer coefficient for a vapour is significantly lower than for a liquid or two-phase fluid, this results in the REFPROP model predicting a superheater area of 4.37 m^2 , compared to 3.34 m^2 for the CAMD-ORC model, thus accounting for the relatively large deviation observed.

Ultimately, the deviation introduced by inputting the cycle parameters from the CAMD-ORC model into the REFPROP heat-exchanger sizing model does not directly represent an issue with the group-contribution transport property prediction methods but is instead a carry-over from the difference between the thermodynamic properties predicted by SAFT- γ Mie within the thermodynamic cycle model and REFPROP. Having said this, neglecting the 2-butene condenser and 1-propene evaporator, the percentage deviation between the CAMD-ORC model and REFPROP for the remaining heat exchangers are all below 5%. These values are very much in line with the percentage deviations observed between the thermodynamic properties (< 5%), and transport properties (< 8%) discussed in Section 3.1. Overall, this gives good confidence in the heat-exchanger sizing model implemented within the CAMD-ORC model.

4. Case studies

As mentioned earlier, the CAMD-ORC framework used here has been used previously to optimise the working fluid and thermodynamic cycle of ORC systems for three different waste-heat streams [49]. In the present work, transport-property group-contribution correlations have been coupled to heat-exchanger sizing models, and the heat-transfer area requirements for a selection of optimal cycles that resulted from the thermodynamic study have been determined in the previous section. The aim of the

case studies explored in the present section, using the same three heat sources as in Ref. [49], is to determine the heat-transfer requirements for a larger group of working fluids and to determine the total specific-investment cost (SIC) for each working fluid. This, in turn, allows optimal cycle configurations to be identified based on thermoeconomic performance indicators. Although the present investigation extends earlier work that focussed on waste-heat applications, the lessons from this study can be also related to the case of power generation from renewable heat [17,75,76].

4.1. Case study assumptions

It should be noted that only basic, non-recuperated, subcritical ORC systems have been considered in the present case studies, despite the CAMD-ORC being successfully extended to, and validated for, alternative cycle architectures within this paper. The is because of the uncertainties that are introduced when considering these novel cycle architectures. Firstly, sizing the heat exchangers for a cycle operating with a working-fluid mixture would require suitable mixing rules to be defined to determine the necessary transport properties. Moreover, there also exist large uncertainties in predicting local heat-transfer coefficients for working-fluid mixtures. Secondly, whilst partially evaporated cycles are an extremely interesting idea from the point of view of maximising power output, commercial expander technologies for two-phase expansion, with a few exceptions [77,78], are not widely available. Therefore, it follows that cost correlations for two-phase expanders do not exist. With this in mind, it follows that a non-recuperated, subcritical ORC system is the easiest to evaluate from a thermoeconomic point of view, and is therefore the best cycle with which to demonstrate the CAMD-ORC framework that has been developed within this paper. Nonetheless, as more research into working-fluid mixtures and partially-evaporated cycles is conducted, the same tool can be used to evaluate these novel cycles, with minimal changes required to the CAMD-ORC framework.

Returning to the case studies, the three heat-sources considered are each defined by a heat-capacity rate ($\dot{m}c_p$) of 4.2 kW/K and by a heat-source temperature of 150 °C, 250 °C and 350 °C respectively. The assumptions for the study are listed in Table 3, whilst the working fluids under consideration are given in Table 4. For all three heat-source temperatures, the heat source is assumed to be the heat-transfer oil Therminol 66® at 1 bar, and the heat sink is water. As stated previously, steady-state operating conditions are assumed, and pressure drops within the heat exchangers and piping are neglected.

The objective of the optimisation is to identify the working fluid and cycle parameters that result in the best thermodynamic performance, and then to assess these optimal systems from an economic perspective. The objective is therefore to maximise power output W_n . For this study, there are five optimisation variables, listed in Table 5, alongside the bounds and constraints for the optimisation.

4.2. Thermodynamic performance

For each working-fluid group in Table 4 a parametric study was completed whereby the number of $-CH_2-$ groups was varied, and the ORC thermodynamic variables were optimised to maximise the power output from system [49]. The results from this parametric study are plotted in terms of the power output in Fig. 6; here C_n refers to the number of carbon atoms in the molecule (*n*-alkane, methyl alkane, 1-alkene or 2-alkene). The optimal working fluids for the three heat source temperatures of 150 °C, 250 °C and 350 °C are *n*-propane (*n*-alkane, $C_n = 3$), 2-pentene (2-alkene, $C_n = 5$) and 2-hexene (2-alkene, $C_n = 6$), corresponding to maximum power

Table 3

Values of the quantities used in the ORC thermodynamic study completed in Ref. [49].

T_{hi} (°C)	$(\dot{m}c_p)_h$ (kW/K)	T_{ci} (°C)	$c_{p,c}$ (kJ/(kg K))	\dot{m}_c (kg/s)	η_p (%)	η_e (%)	$PP_{h,min}$ (°C)	$PP_{c,min}$ (°C)	$P_{1,min}$ (bar)
150, 250, 350	4.2	15	4.2	5.0	70	80	10	5	0.25

Table 4

Working-fluid groups considered within this study.

<i>n</i> -alkanes	methyl alkanes	1-alkenes	2-alkenes
$CH_3-(CH_2)_n-CH_3$	$(CH_3)_2-CH-(CH_2)_n-CH_3$	$CH_2=CH-(CH_2)_n-CH_3$	$CH_3-CH=CH-(CH_2)_n-CH_3$

Table 5

Bounds for the optimisation variables and constraints applied during the optimisation.

Variable	Lower bound	Upper bound	Unit	Constraints
T_1	288	353	K	$T_{ho} - T_2 \geq PP_{h,min}$
p_r	0.001	0.85	–	$T_{hp} - T_2 \geq PP_{h,min}$
z	1.0	2.0	–	$T_{hi} - T_3 \geq PP_{h,min}$
PP_h	10	200	K	$T_1 - T_{cp} \geq PP_{c,min}$
$-(CH_2)_n-$	0	10	–	$T_4 - T_{cp} \geq PP_{c,min}$

outputs of 35.2, 136.7 and 219.0 kW respectively. The corresponding thermal cycle efficiencies are 9.7%, 16.9% and 17.8% respectively.

The optimal cycles that correspond to the maximum power are explored in Fig. 7, in which are displayed three of the cycles ($C_n = 4, 5$ and 6) for the *n*-alkane, 250 °C case-study on a *T*-*s* diagram.

When $C_n = 4$, the evaporation temperature, and therefore evaporation pressure, is constrained by the critical temperature since we are only considering subcritical cycles. This results in an optimal cycle with a high reduced pressure and a large amount of superheating, since the high-temperature heat can only be absorbed by the cycle by increasing the working-fluid temperature whilst maintaining the same pressure. This introduces the need for an additional heat exchanger, namely the superheater, in addition to increasing the irreversibilities within the heat-addition process, owing to the increased temperature difference between the heat source and working fluid in the evaporation and superheating regions, resulting in a 16% reduction in the power output compared to the optimal cycle. It is also noted that the minimum allowable evaporator pinch point is observed at the preheater inlet in addition to the evaporator inlet. This corresponds to the lowest heat-

source outlet temperature, indicating that the ORC absorbs the maximum amount of heat from the available heat source. Arguably, the thermodynamic performance of the $C_n = 4$ cycle could be improved by increasing the evaporation pressure above the critical pressure, and thus operate a transcritical cycle. However, it is worth noting that higher evaporation pressures lead to more expensive system components, and this can make subcritical cycles more attractive from an economic perspective [79]. Nonetheless, future efforts should extend the existing CAMD-ORC model to transcritical cycles.

In comparison, when $C_n = 6$, the critical temperature of the working fluid is increased, which means the evaporation temperature is no longer constrained by the critical temperature. Instead, the evaporation temperature, and therefore evaporation pressure, is constrained by the heat-source temperature profile, and the imposed pinch point at the evaporator inlet. This results in no superheating and a lower reduced evaporator pressure. Whilst the former means a superheater is no longer required, the latter results in a larger latent-heat of evaporation, which impacts the cycle in two ways. Firstly, the larger latent-heat means that a larger proportion of the heat-addition process occurs at a constant temperature, which increases the average temperature difference between the heat source and working fluid, resulting in more irreversibility. Secondly, the larger latent-heat also means that the preheater inlet is no longer pinched, which means this cycle absorbs less heat from the heat source. These combined effects result in a 13% reduction in power output compared to the optimal cycle.

Finally, when $C_n = 5$, the maximum power is obtained. This cycle has a high-reduced pressure, minimal superheating, and the minimum allowable pinch point is once again observed at both the preheater inlet and the evaporation inlet. Overall, this means that

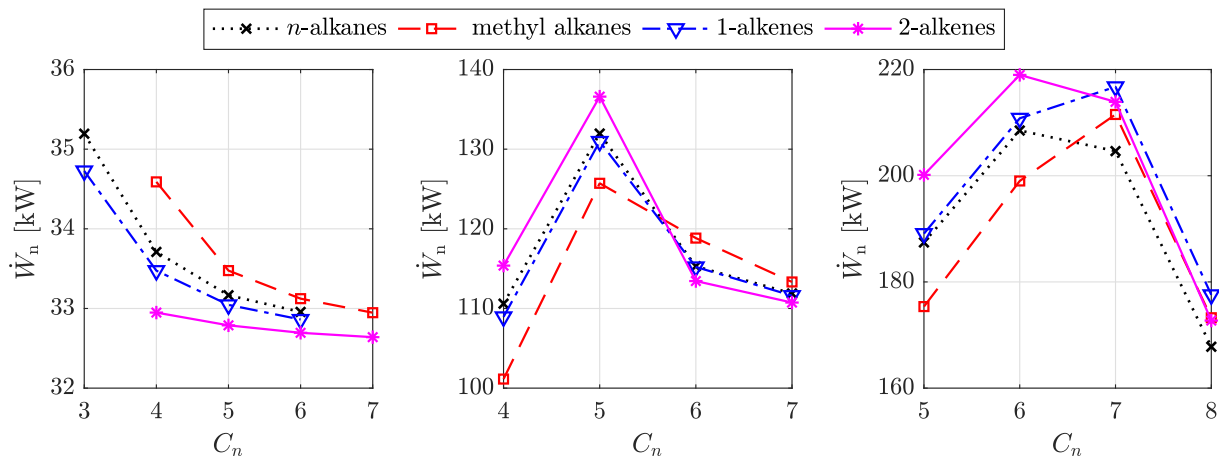


Fig. 6. Optimal net power output from an ORC system operating with different hydrocarbon working fluids. Results are plotted against the number of carbon atoms C_n in the molecule (*n*-alkane, methyl alkane, 1-alkene or 2-alkene, as indicated). From left to right: $T_{hi} = 150$ °C, 250 °C, 350 °C.

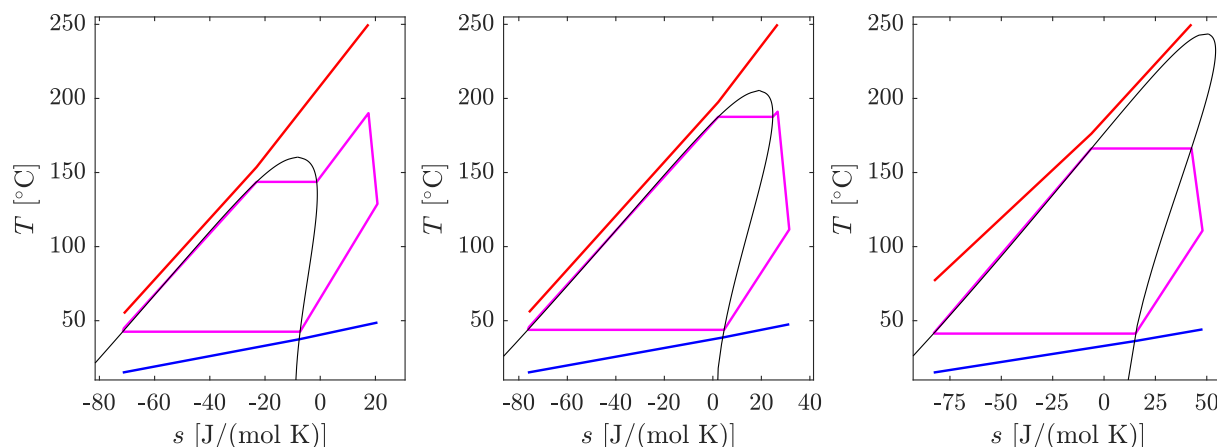


Fig. 7. T-s plots for three cycles from the *n*-alkane, 250 °C case-study. From left to right: $C_n = 4$ (*n*-butane), 5 (*n*-pentane) and 6 (*n*-hexane). The red and blue lines represent to the heat-source and heat-sink streams, the magenta lines correspond to the thermodynamic power cycle and the black line indicates the working-fluid saturation dome. (For interpretation of the references to colour in this figure legend, the reader is referred to the Web version of this article.)

the ORC absorbs the maximum amount of heat possible, whilst a low latent heat of vaporisation, and minimal superheating results in the majority of heat-transfer occurring during in the preheating region. This minimises irreversibilities within the heat-addition process, and results in the maximum power output.

The effect of the working fluid, in terms of the number of carbon atoms, on the evaporator and condenser thermal load has been reported in Figs. 8 and 9 respectively. For the evaporator, \dot{Q}_{ph} , \dot{Q}_{ev} and \dot{Q}_{sh} refer to the preheating, two-phase evaporation, and superheating loads respectively, and for the condenser \dot{Q}_{ds} and \dot{Q}_{co} refer to the desuperheating and two-phase condensation loads respectively. In Figs. 8 and 9, only the results for one particular working-fluid family have been presented for each heat-source temperature, and this corresponds to *n*-alkane family for the 150 °C heat source, and the 2-alkene family for both the 250 and 350 °C heat sources. However, there was not observed to be a large difference in the breakdown in the heat-exchanger load as the working-fluid family is changed, and therefore the discussion in the following paragraphs is relevant to all of the families considered here.

In terms of the evaporator load a number of observations can be made. Firstly, for the 150 °C and 250 °C heat-source temperatures there is a clear link between maximising the power output and

increasing the preheater load, with both parameters showing the same trend as C_n is increased. Moreover, for molecules that are less complex than the optimal fluid it is always necessary to have superheating, whilst for molecules that are more complex than the optimal fluid the evaporation load increases. Furthermore, it is observed that as the heat-source temperature increases the proportion of heat-addition that occurs within the preheater increases. More specifically, for the 150 °C heat-source temperature the preheater accounts for between 32.0% and 44.3% of the total evaporator load, whilst for the 350 °C heat-source temperature, the preheater accounts for between 49.2% and 83.8% of the total evaporator load, depending on the fluid.

Referring to Fig. 9, similar observations for the condenser load can be observed. Firstly, for the 150 °C and 250 °C heat-source temperatures, it is observed that maximising the power output also corresponds to the largest condensation load, although the difference between the different fluids is not as significant. It is also observed that in general the less complex molecules result in the highest desuperheater loads. This was to be expected as these cycles include superheaters, and therefore the working-fluid conditions at the outlet of the expander will be more superheated than the optimal cycles. In terms of the effect of the heat-source temperature on the distribution of the condenser load, it is observed

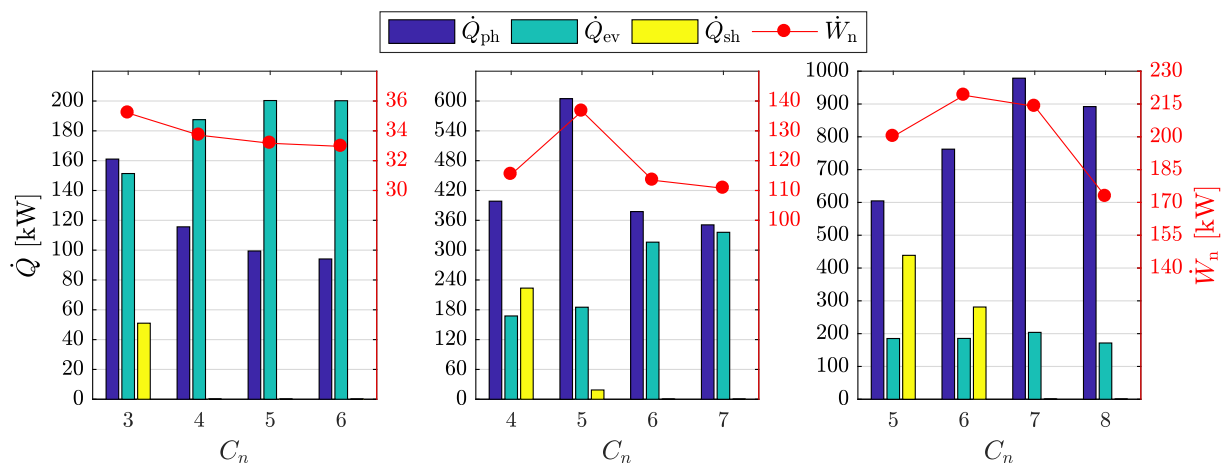


Fig. 8. Breakdown of evaporator load for an optimal ORC system operating with different hydrocarbon working fluids. From left to right: $T_{hi} = 150$ °C (*n*-alkane family); $T_{hi} = 250$ °C (2-alkene family); $T_{hi} = 350$ °C (2-alkene family).

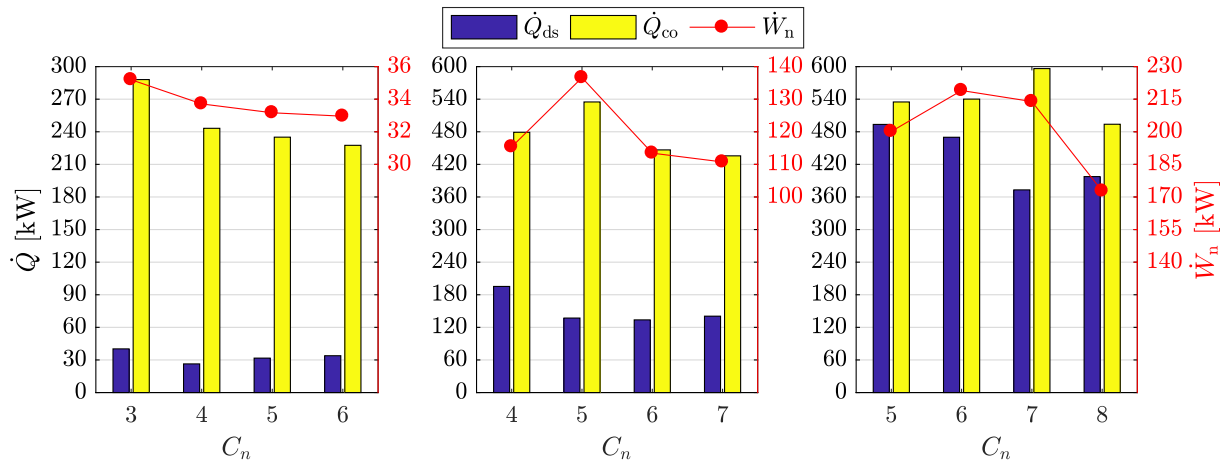


Fig. 9. Breakdown of condenser load for an optimal ORC system operating with different hydrocarbon working fluids. From left to right: $T_{hi} = 150\text{ °C}$ (n-alkane family); $T_{hi} = 250\text{ °C}$ (2-alkene family); $T_{hi} = 350\text{ °C}$ (2-alkene family).

that increasing the heat-source temperature results in a larger proportion of the heat rejection occurring during the desuperheater stage. For example, for the 150 °C the desuperheater accounts for between 9.8% and 13.0% of the total condenser load, whilst for the 350 °C heat-source temperature this increases to between 38.5% and 48%. This effect can be explained by considering the behaviour of the saturation dome of hydrocarbon working fluids as the critical temperature is increased. In general, the saturation dome of a working fluid with a higher critical temperature will have a larger overhang when viewed on a T - s diagram. Therefore, expansion will result in a larger amount of superheat at the expander outlet. Moreover, this effect becomes more pronounced as the pressure ratio is increased, as is the case when the heat-source temperature increases. The increased desuperheater load for the 350 °C heat-source temperature also has an effect on the thermal efficiency, as increased desuperheating raises the average temperature of heat rejection. This, coupled to higher condensation temperatures for the 350 °C systems owing to the fixed heat-sink heat capacity rate, means that despite the 350 °C systems producing significantly more power, the thermal efficiencies are similar to the 250 °C systems. More specifically, the thermal efficiencies range between 9.7% and 11.2% for the 150 °C systems, 14.6% and 16.9% for the 250 °C systems and 16.2% and 18.1% for the 350 °C systems.

4.3. Component sizing performance

Following from the thermodynamic analysis, the required heat-transfer areas for the evaporator and condenser can be obtained using the heat-exchanger sizing model based on group-contribution transport properties. Breakdowns of the evaporator and condenser heat-transfer area requirements are shown in Figs. 10 and 11 for the same working fluids and cycles considered in Figs. 8 and 9. For the evaporator, A_{ph} , A_{ev} and A_{sh} refer to the preheating, two-phase evaporation, and superheating areas, and for the condenser A_{ds} and A_{co} refer to the desuperheating and two-phase condensation areas, respectively.

Unsurprisingly, for each heat-source temperature, the cycle with the highest power output results in the highest evaporator heat-transfer area requirement, corresponding to 78.8 m^2 , 264.1 m^2 and 313.6 m^2 for the n -propane, 2-pentene and 2-hexene cases, respectively. However, it is observed that whilst selecting a different working fluid will cause a reduction in the power output, the reduction in the heat-transfer area can be significant. For

example, for the three heat-source temperatures, if C_n is increased by one, the power output is reduced by 4.2%, 16.9% and 2.3%, but this also corresponds to a reduction in the total evaporator area by 35.6%, 66.1% and 48.1%, respectively. Therefore, it is clear that a trade-off between higher power output and size/cost exists that must be considered when selecting the most suitable working fluid for a particular application.

Considering the breakdown of the evaporator heat-transfer area, it is observed that in general the preheater section accounts for the largest percentage of the required area. This was to be expected from considering the evaporator load breakdown (Fig. 8), but is further exaggerated since the overall heat-transfer coefficient for two-phase evaporation is generally higher than it is for single-phase heat transfer, meaning a larger area is required to transfer the same amount of heat. For all the fluids evaluated, the preheating overall heat-transfer coefficient ranged between 176 and $305\text{ W}/(\text{m}^2\text{ K})$, whilst the two-phase evaporation overall heat-transfer coefficient ranged between 268 and $591\text{ W}/(\text{m}^2\text{ K})$. Adding to this, the minimum pinch point is recorded in the preheater section reducing significantly the log-mean temperature difference between the two working fluids. This results in an increase of the area requirements of the preheater in comparison to the two-phase evaporating section, even for very similar heat-transfer loads. A case in point is given by fluids with $C_n = 3$ at the 150 °C heat-source temperature that have similar preheater and evaporator loads (Fig. 8), but the preheater area required is more than double the respective one for the evaporator section (Fig. 10). Similar findings are observed for fluids with $C_n = 7$ at 250 °C heat-source temperature. Referring to the results in Fig. 10, for the 150 °C heat-source temperature the preheater accounts for between 43.2% and 66.4% of the total evaporator area, whilst for the 350 °C heat-source temperature, the preheater accounts for between 89.5% and 96.4% of the total evaporator area, depending on the fluid.

For the condenser heat-transfer area requirements, similar observations to those made when evaluating the condenser load are found; namely that, with the exception of the $C_n = 5$, 350 °C case study, the thermodynamic optimal cycles result in the largest heat exchangers. More specifically, for the n -propane, 2-pentene and 2-hexene cases, the total condenser areas are 37.6 m^2 , 46.4 m^2 and 51.1 m^2 respectively. Interestingly though, it is observed that the required condenser area doesn't increase significantly as the heat-source temperature increases. This is attributed to the higher temperature differences between the heat sink, and the expander outlet temperature and the condensation temperature as the heat-

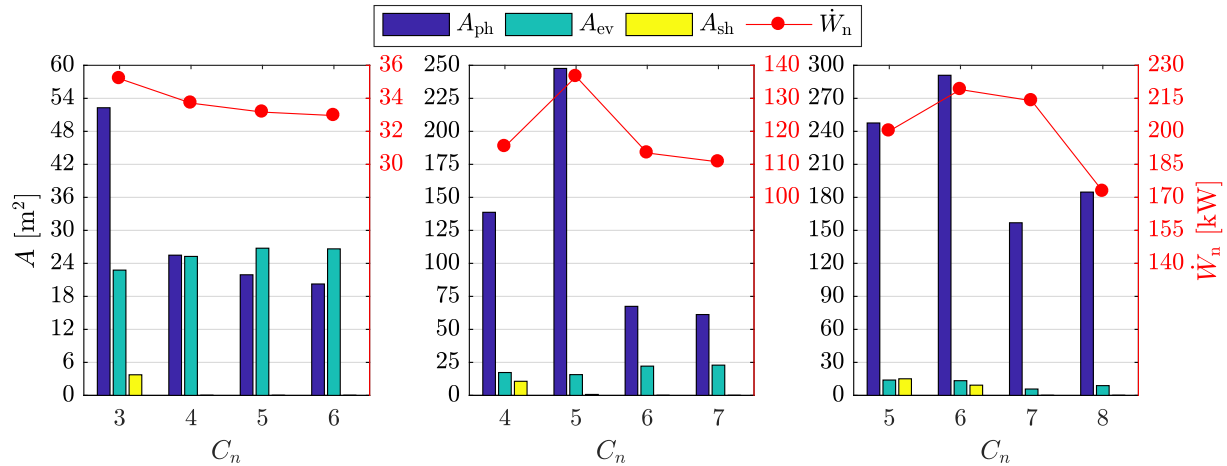


Fig. 10. Breakdown of evaporator heat-transfer area requirements for an optimal ORC system operating with different hydrocarbon working fluids. From left to right: $T_{hi} = 150\text{ }^{\circ}\text{C}$ (n -alkane family); $T_{hi} = 250\text{ }^{\circ}\text{C}$ (2-alkene family); $T_{hi} = 350\text{ }^{\circ}\text{C}$ (2-alkene family).

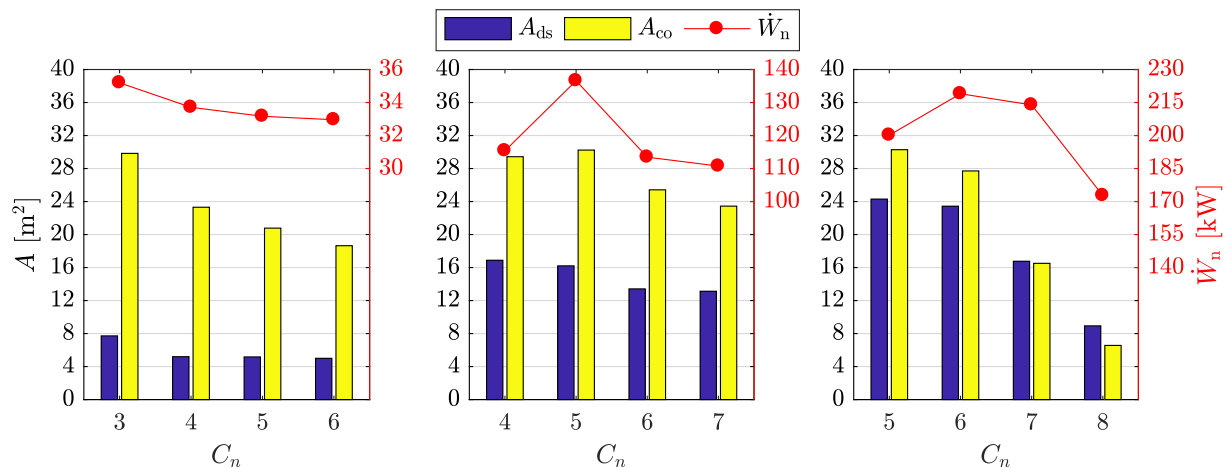


Fig. 11. Breakdown of condenser heat-transfer area requirements for an optimal ORC system operating with different hydrocarbon working fluids. From left to right: $T_{hi} = 150\text{ }^{\circ}\text{C}$ (n -alkane family); $T_{hi} = 250\text{ }^{\circ}\text{C}$ (2-alkene family); $T_{hi} = 350\text{ }^{\circ}\text{C}$ (2-alkene family).

source temperature increases. For example, for the cycles reported in Fig. 11, the condensation temperatures range between 303.8 K and 306.7 K for the 150 °C heat source, 313.7 K and 318.5 K for the 250 °C heat source and 318.5 K and 354.5 K for the 350 °C heat source. This significant increase in the condensation temperature increases the log-mean temperature difference, and therefore heat flux, in the condenser resulting in much lower heat-transfer area requirement for a similar load. It is also worth noting that the significant increase in the condensation temperature for the $C_n = 8$, 350 °C case, is because a minimum condensation pressure constraint is applied (0.25 bar) during the optimisation. In fact, for both the $C_n = 7$ and $C_n = 8$ cases for this heat-source temperature the condensation pressure is actually equal to the minimum allowable condensation pressure. Therefore, a lower condensation temperature cannot be achieved without violating this constraint. Not only does this have a significant effect on the condenser area, as observed in Fig. 11, it also has an impact on the evaporator area requirements, as the minimum allowable heat-source temperature must also increase, which in turn moves the evaporator pinch-point to the preheating inlet, rather than at the start of evaporation.

Comparing the breakdown of the condenser heat-transfer area requirements, and the breakdown of the condenser load, it is observed that the breakdown of the load and area are fairly similar.

The desuperheater area accounts for a slightly larger proportion of the total condenser area, compared to the desuperheating load, and this can again be attributed to the higher overall heat-transfer coefficients for two-phase heat transfer compared to the single-phase heat transfer. For all the fluids evaluated, the desuperheating overall heat-transfer coefficients ranged between 385 and 518 W/(m² K), whilst for two-phase condensation it ranged between 926 and 1450 W/(m² K).

The total heat-transfer area requirements (*i.e.*, total evaporator area A_h , and total condenser area A_c) for each heat-source temperature and each working fluid considered within this study are plotted in Fig. 12. Considering this figure, and referring back to Fig. 6, it is clear that the optimal thermodynamic cycles always result in the largest heat exchangers, and this is particularly true for the 150 °C and 250 °C heat-source temperatures. The reason can also be explained by reconsidering Fig. 7, and the accompanying discussion. That is to say that the optimal thermodynamic cycle results in a large preheating load, which means a large proportion of the available heat is absorbed by the cycle which increases power output. However, this heat transfer occurs under a small temperature difference, resulting in a large heat-transfer area requirement.

Finally, to conclude this section it is useful to evaluate the expander volume ratio, defined as the ratio of the inlet and out

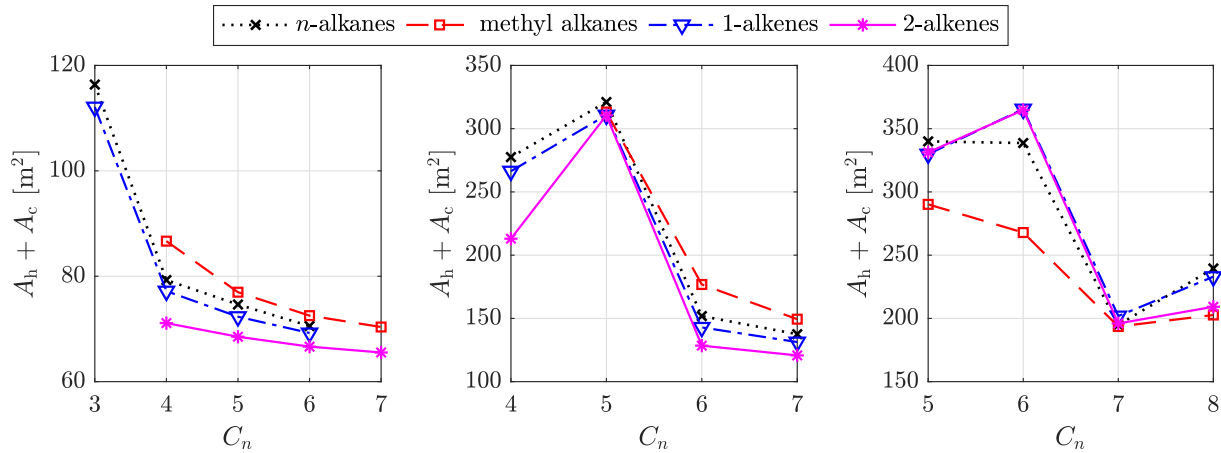


Fig. 12. Total heat-transfer area requirements for each cycle previously identified in Fig. 6. From left to right: $T_{hi} = 150\text{ }^{\circ}\text{C}$, $250\text{ }^{\circ}\text{C}$, $350\text{ }^{\circ}\text{C}$.

densities (i.e., ρ_3/ρ_4). For the $150\text{ }^{\circ}\text{C}$ and $250\text{ }^{\circ}\text{C}$ systems, the volume ratio increases as the number of carbon atoms is increased, but is not found to vary significantly when comparing the different fluid families. More specifically, the expansion ratios range between 3.1 and 9.7 for the $150\text{ }^{\circ}\text{C}$ systems, and 6.7 and 36.1 for the $250\text{ }^{\circ}\text{C}$ systems. For the $350\text{ }^{\circ}\text{C}$ systems, the volume ratio increases until the condensation pressure constraint comes into play ($C_n > 7$), after which it reduces. For these systems the volume ratio is found to range between 17.5 and 162. Ultimately, the volume ratios for the $150\text{ }^{\circ}\text{C}$ and $250\text{ }^{\circ}\text{C}$ systems can be accommodated by a single-stage radial turbine, or a suitable volumetric expander, whilst it is likely that the $350\text{ }^{\circ}\text{C}$ systems, operating with working fluids of increasing molecular complexity, would be more suited to multi-stage designs. Therefore, whilst it is reiterated that expander design is not a focus of this paper, future research should account for the effect of the volume ratio on the expander selection, design and associated costs.

4.4. Thermoeconomic results

Clearly, there is a trade-off between thermodynamic performance and the size of the system components. Using the known heat-transfer areas, the pump work and expander work for each cycle, the cost correlations described in Section 2.4 can be used to obtain the specific-investment cost (SIC) (Fig. 13). Within this study, the heat-source heat capacity rate has been fixed at 4.2 kW/K and

the heat-source temperature has been varied, which as observed from Fig. 6, has led to different sized systems for each heat-source temperature. Therefore, when evaluating the cost of the system there are two factors at play; the size of the system, and the heat-source temperature. On the one hand, larger systems will be associated with lower relative costs for the manufacturing of components, owing to economy-of-scale effects, which will reduce the SIC. On the other hand, higher temperature systems will be associated with higher power outputs, owing to higher thermal efficiencies, which will also reduce the SIC. Therefore, as one would expect, it is observed in Fig. 13 that the lowest temperature and smallest systems ($150\text{ }^{\circ}\text{C}$) correspond to the highest SIC whilst the highest temperature and largest systems ($350\text{ }^{\circ}\text{C}$) correspond to the lowest SIC. Unfortunately, it is difficult to determine what fraction of the reduction in SIC for the 250 and $350\text{ }^{\circ}\text{C}$ systems can be attributed to the increase in the system size, and what fraction can be attributed to the increase in the heat-source temperature. Future research should attempt to decouple these two effects, for example by scaling the heat-source capacity rate such that the power output from each system is the same.

Referring back to Fig. 13, it is observed that for each heat-source temperature and hydrocarbon family, there appears to be a particular working fluid that will minimise the SIC. For the $150\text{ }^{\circ}\text{C}$, $250\text{ }^{\circ}\text{C}$ and $350\text{ }^{\circ}\text{C}$ heat-source temperatures the minimum SICs are 5620, 2760 and 2070 £/kW respectively, and these are found for $C_n = 7$ (isoheptane), $C_n = 5$ (2-pentene) and $C_n = 7$ (2-heptene)

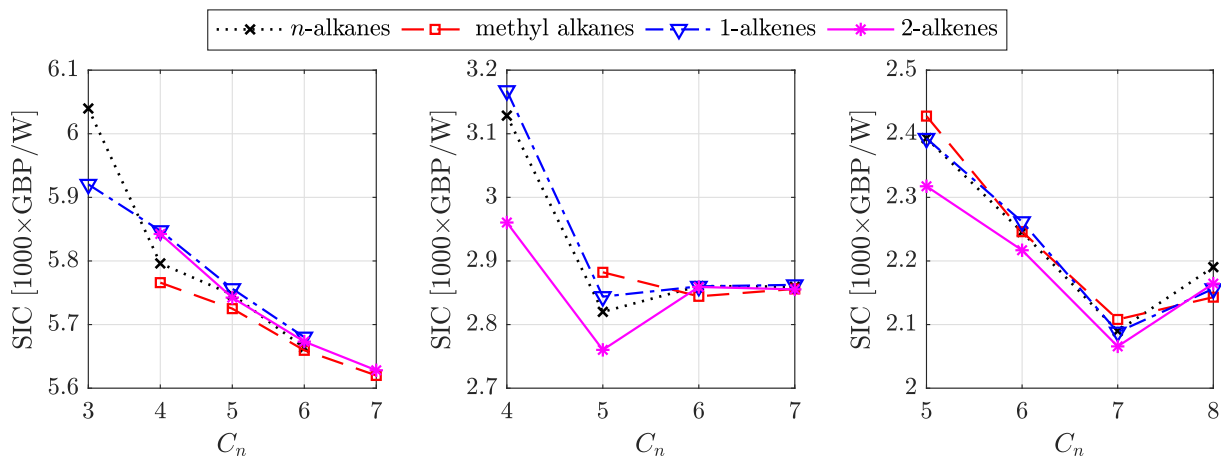


Fig. 13. Specific investment cost (SIC) in £/kW for each optimal cycle previously identified in Fig. 6. From left to right: $T_{hi} = 150\text{ }^{\circ}\text{C}$, $250\text{ }^{\circ}\text{C}$, $350\text{ }^{\circ}\text{C}$.

respectively. It should be noted that within the CAMD-ORC model there is no consideration of the order of the functional groups within the molecule. Therefore, isoheptane refers to either 2-methyl hexane or 3-methyl hexane, depending on the location of the $-\text{CH}$ group. For the 250 °C heat source 2-pentene is found to both maximise the power output and minimise the SIC, and is therefore identified as the optimal working fluid. However, for the other two heat sources, different working fluids are identified based on whether a thermodynamic or thermoeconomic performance metric is used.

Of particular interest, are the results for the 350 °C heat source, which suggest that in terms of minimising the SIC, it could be beneficial to use a working fluid with $C_n = 7$. The four fluids considered with $C_n = 7$ have condensation temperatures ranging between 49.4 °C (methyl alkane) and 56.8 °C (2-alkene), with corresponding pinch points at the start of evaporation of 53.1 °C and 39.5 °C respectively. This results in relatively large temperature differences within the heat exchangers, thus reducing the heat-transfer area requirement and therefore cost. Lowering C_n reduces both the condensation temperature and the pinch point, resulting in better performance but much higher costs. On the other hand, increasing C_n to 8 corresponds to condensation temperatures between 74.5 °C (methyl alkane) and 81.7 °C (*n*-alkane) resulting in a significant reduction in performance. It is also interesting to note that there is only a small difference between the optimal SIC for each fluid family, with the optimal SIC ranging between 2065 £/kW (2-alkene) and 2108 £/kW (methyl alkane), which corresponds to a 2.1% increase in the SIC when using a methyl alkane compared to a 2-alkene. Ultimately, this suggests that in this case the molecular complexity (*i.e.*, the number of carbon atoms) is more critical than the specific molecular structure.

In order to confirm that the SIC values obtained in this study are representative of actual ORC systems, our results are compared to SIC data available in the literature. More specifically, Lemmens [66] collated cost data for ORC systems designed for different applications, including biomass, solar, geothermal and waste-heat recovery. In Fig. 14, the results from the current study are compared to the data reported by Lemmens for waste-heat recovery applications, adjusted from €₂₀₁₄ to £₂₀₁₇ using the CEPCI values for 2014 (576.1) and 2017 (562.1), and the current exchange rate (€ 1 = £ 0.87).

From Fig. 14 it is observed that the SIC values obtained within this paper match well with those reported within the literature,

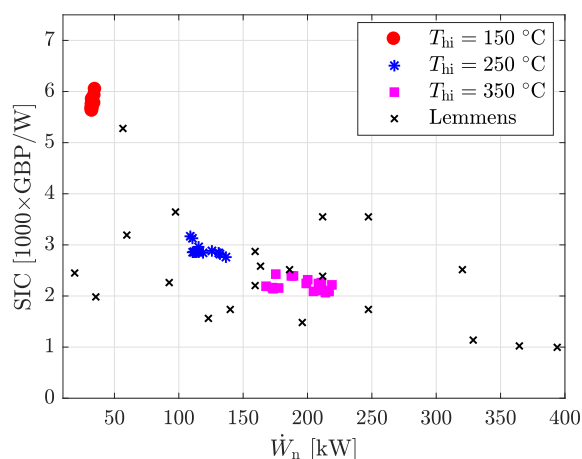


Fig. 14. Effect of the system size (in kW) on the specific-investment cost in £/kW. The results from this study for the three different heat-source temperatures are compared to SIC data reported by Lemmens [66].

and this is particularly true for the 250 and 350 °C systems. The SIC values obtained for the 150 °C systems follow the general trend in that SIC increases as the system size reduces, but are slightly higher than SIC values taken from the literature. However, it is worth noting that Lemmens did not consider the effect of heat-source temperature on the system economics. In reality, a low-temperature heat source will lead to a lower thermal efficiency, and therefore it is reasonable to assume a 50 kW, 150 °C system will have a higher SIC than a 50 kW, 250 °C system. Therefore, the heat-source temperature is actually a third dimension, which is not reported Fig. 14. With this in mind, it is reasonable to accept the SIC values obtained for the 150 °C systems.

Alongside considering the SIC values obtained for the systems, it is also interesting to consider the breakdown in the system cost, and this is reported in Fig. 15 for the same working fluids previously evaluated in terms of the heat-exchanger load and heat-transfer area requirements for the evaporator and condenser. Again, it is noted that the results reported in this figure are representative of the results obtained for each working-fluid family.

Firstly, it is noted that for all the cases considered the pump only accounts for a very small fraction (<2.3%) of the total system cost. Furthermore, the evaporator and condenser both account for a similar fraction of the overall costs, which corresponds to approximately ~35%, ~20% and ~15% of the total system cost in the 150 °C, 250 °C and 350 °C heat-source temperature cases, respectively. However, the most obvious observation from Fig. 15 concerns the significant fraction of the total cost that is accounted for by the expander at the higher heat-source temperatures. This behaviour can, in part, be explained by the higher ORC system thermal efficiencies at the higher heat-source temperatures, and the correspondingly greater fraction of the heat that is exchanged between the system and the heat source/sink that is converted into power, and which therefore requires a larger expander with a higher power output and a larger generator for the same heat-exchanger duty.

Another possible reason for such a large cost estimate for the expander could relate to the suitability of the expander cost correlation for ORC systems. Arguably, within an ORC system, the cost of the expander is the largest unknown, particular for small-scale systems below a few-hundred kW, as the commercialisation of these systems is still in its infancy. For this study, the material factor F for the expander, which accounts for component manufacturing, was set to 3.5 based on recommendations within the literature. However, it should be noted that these correlations were not developed specifically for ORC expanders, but instead originate from the chemical industry, and should be used for comparing alternative system configurations and working fluid performance, where the relative results are more important than the absolute cost figures.

Despite possible uncertainties with the cost correlations, referring back to Fig. 14 it has been shown that the SIC values predicted by the CAMD-ORC are in good agreement with values reported within the literature. Moreover, it should be stated the primary aim of this paper has been to develop a CAMD-ORC framework that can be used to identify novel ORC architectures from a thermoeconomic perspective. Therefore, the cost correlations applied within this framework can be easily adapted as the ORC market continues to grow, and more cost information on the system components becomes available.

5. Further economic considerations

In this paper we have assumed a constant heat-source mass-flow rate, however, in most real applications this heat stream will be variable both in flow rate and temperature, depending on the

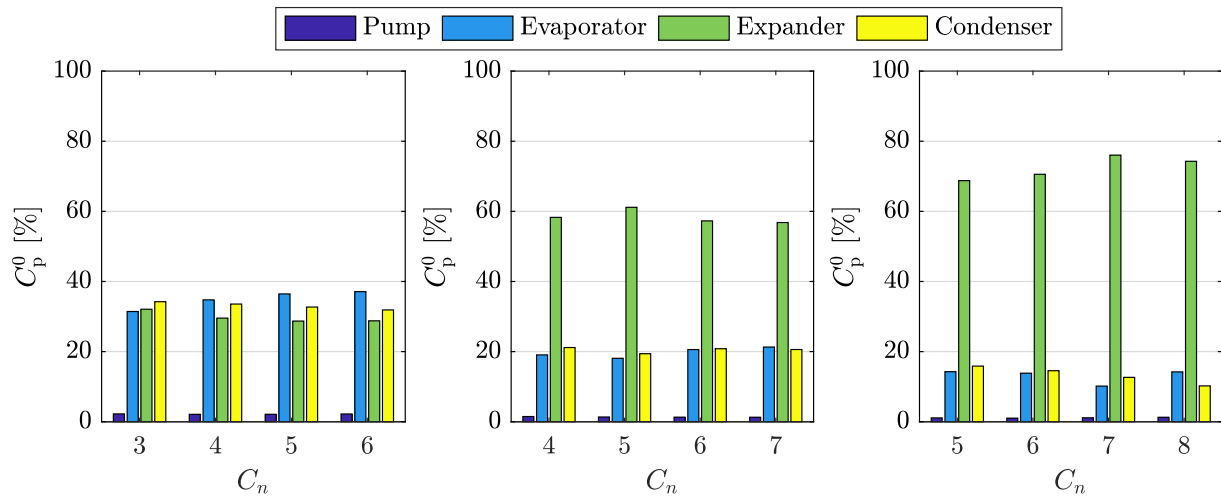


Fig. 15. Breakdown of the total system cost for different hydrocarbon working fluids and heat-source temperatures. From left to right: $T_{hi} = 150$ °C (n-alkane family); $T_{hi} = 250$ °C (2-alkene family); $T_{hi} = 350$ °C (2-alkene family).

application (e.g., intermittent waste heat from industrial processes, variable solar energy, seasonal biomass supply and so on). Moreover, this heat stream may be used not only to generate electricity, but also to match on-site heating/cooling demands at different temperature levels, according to the typology of the energy demand (i.e., residential, commercial or industrial). In some cases, this means that the ORC system configuration should be optimised to maximise the global energy-conversion efficiency, instead of the electrical efficiency. This could include using the discharged heat from the ORC cooling stream for further on-site cogeneration, or accounting for smart operating strategies to modulate or switch on/off the system in order to follow the heat demand. In addition, the intermittency of the heat source introduces further trade-offs in the optimal thermal-storage capacity, considering that thermal storage could increase the system's operating hours, but also increase costs, as well as reduce the available input temperature and, in turn, the electricconversion efficiency.

The overall thermodynamic performance of the ORC system should be optimised for different outlet temperatures of the cooling stream. A higher outlet temperature increases the energy of the heat-sink stream but decreases the power output of the expander. Conversely, a low outlet temperature allows for a high power output, but has a low potential to heat buildings or match other industrial thermal energy demand. Moreover, the waste-heat supply and the low temperature heating demand profiles are often not well matched. This means that, without a proper thermal storage system, cogenerated heat from the ORC-CHP can be wasted over large periods of the year. This is particularly true when waste heat availability makes profitable a base-load CHP operation, instead of thermal load following operations. The optimal working fluid for a given temperature of heat demand identified from an optimisation procedure may not be the optimal one if the heating demand is affected by high temporal variations, and does not match the CHP output profile. For this reason, the influence of heat-demand profile on optimal working fluid selection and global CHP conversion efficiency should be taken into account.

Some of these trade-offs have been addressed in recent literature, such as in Ref. [80], which includes the optimisation of the ORC working fluid as the temperature of heat demand and the operational model change. Other studies compare levelized costs of energy and profitability of ORC configurations as a function of intermittency of heat source [81], and thermal-energy storage size and intermittency of the waste-heat [82] or solar-energy [83] input.

Operational strategies and the dynamics of heat supply-energy demand have also been studied [84], in addition to the possibility to match electrical, heating and cooling demands via smart operation of the ORC system coupled to heat sources at different temperature levels [85].

In light of these considerations, an important next step should consider system operational strategies for best thermoeconomic performance (i.e., minimising the levelised-cost of energy instead of the SIC), the ORC cooling stream temperature, the matching of heat discharged from the ORC to on-site heat demand, and the dynamics between heat sources and energy demand. Moreover, the effect of the condensing temperature on the condenser size, and in turn, the SIC needs further investigation in order to understand the sensitivity of the system to this parameter. Finally, studies should address the broader benefits in terms of the energy systems flexibility that could be provided by such distributed energy technologies.

6. Conclusions

The identification of new working fluids that can improve thermodynamic performance and reduce system costs while meeting increasingly restrictive environmental legislation, along with the determination of novel and optimal ORC system architectures and designs based on combined thermoeconomic performance indicators are key steps toward improving the economic viability of ORC technology and enabling its widespread uptake for power generation or cogeneration from renewable or recovered waste-heat in many applications. The aim of this paper has been to incorporate, for the first time, thermoeconomic analysis, through component sizing and suitable costing correlations, into a CAMD-ORC framework that combines working-fluid design and thermodynamic ORC system optimisation based on the SAFT- γ Mie equation of state.

Discretised heat-exchanger sizing models based on group-contribution methods for determining transport properties have been developed and used to size the evaporator and condenser of optimised ORC systems, and the resulting system specific-investment costs (SICs) that include the costs of these components as well as the pump and expander have been determined using suitable cost correlations. In addition, the CAMD-ORC framework has been extended to allow the consideration of novel cycle architectures, including recuperated and partially-evaporated cycles, and also

cycles operating with working-fluid mixtures. Both the thermodynamic model and heat-exchanger sizing models have been validated against data from NIST REFPROP, and a good agreement is found for the fluids and cases considered. The largest deviations observed in the heat-exchanger area were +18% and –13% when sizing the condenser for 2-butene and the evaporator for propene, respectively. These relatively small deviations confirm the suitability of the group-contribution transport property prediction methods used in this work.

From a series of case studies that span a wide range of conditions, it is found that working fluids that maximise the power output from ORC systems generally have the highest heat-exchanger area requirements. Therefore, working-fluid selection based on SIC minimisation can result in different optimal working fluids to those identified from an optimisation that considers power output or other common thermodynamic objective functions. Specifically, for the three heat-source temperatures considered in this work (150 °C, 250 °C and 350 °C, each with $\dot{m}c_p = 4.2$ kW/K, corresponding to small- to medium-scale applications) the ORC systems with the lowest SIC have isoheptane, 2-pentene and 2-heptene as their working fluids, with SICs of £5620, £2760 and £2070 per kW respectively. The corresponding power outputs for these ORC systems are 32.9 kW, 136.6 kW and 213.9 kW, which are 6.38%, 0.0% and 2.32% lower than the power outputs obtained for working fluids that maximise the system power output. This also corresponds to a reduction in the SIC of 6.95%, 0.0% and 6.82%. Overall, with three optimal working fluids having been identified for each of the three different heat-source temperatures, these results demonstrate the importance of considering thermoeconomic performance within the CAMD-ORC framework.

Acknowledgements

This work was supported by the UK Engineering and Physical Sciences Research Council (EPSRC) [grant number EP/P004709/1, and award number 1855813]. The authors would also like to acknowledge the Imperial College President's PhD Scholarship Scheme and the Climate-KIC PhD Added Programme for funding this research. Data supporting this publication can be obtained on request from cep-lab@imperial.ac.uk.

References

- Markides CN, Smith TCB. A dynamic model for the efficiency optimization of an oscillatory low grade heat engine. *Energy* 2011;36(12):6967–80. <https://doi.org/10.1016/j.energy.2011.08.051>.
- Solanki R, Galindo A, Markides CN. Dynamic modelling of a two-phase thermofluidic oscillator for efficient low grade heat utilization: Effect of fluid inertia. *Appl Energy* 2012;89(1):156–63. <https://doi.org/10.1016/j.apenergy.2011.01.007>.
- Solanki R, Mathie R, Galindo A, Markides CN. Modelling of a two-phase thermofluidic oscillator for low-grade heat utilisation: Accounting for irreversible thermal losses. *Appl Energy* 2013;106:337–54. <https://doi.org/10.1016/j.apenergy.2012.12.069>.
- Markides CN, Osuolale A, Solanki R, Stan GBV. Nonlinear heat transfer processes in a two-phase thermofluidic oscillator. *Appl Energy* 2013;104:958–77. <https://doi.org/10.1016/j.apenergy.2012.11.056>.
- Palanisamy K, Taleb AI, Markides CN. Optimizing the non-inertive-feedback thermofluidic engine for the conversion of low-grade heat to pumping work. *Heat Transf Eng* 2015;36(14–15):1303–20. <https://doi.org/10.1080/01457632.2015.995014>.
- Taleb AI, Timmer MAG, El-Shazly MY, Samoilov A, Kirillov VA, Markides CN. A single-reciprocating-piston two-phase thermofluidic prime-mover. *Energy* 2016;104:250–65. <https://doi.org/10.1016/j.energy.2016.02.113>.
- Oyewunmi OA, Kirmse CJW, Haslam AJ, Müller EA, Markides CN. Working-fluid selection and performance investigation of a two-phase single-reciprocating-piston heat-conversion engine. *Appl Energy* 2017;186:376–95. <https://doi.org/10.1016/j.apenergy.2016.05.008>.
- Kirmse CJW, Oyewunmi OA, Taleb AI, Haslam AJ, Markides CN. A two-phase single-reciprocating-piston heat conversion engine: Non-linear dynamic modelling. *Appl Energy* 2017;186:359–75. <https://doi.org/10.1016/j.apenergy.2016.05.140>.
- Kirmse CJW, Oyewunmi OA, Haslam AJ, Markides CN. Comparison of a novel organic-fluid thermofluidic heat converter and an organic Rankine cycle heat engine. *Energies* 2016;9(7):479. <https://doi.org/10.3390/en9070479>.
- Bao J, Zhao L. A review of working fluid and expander selections for organic Rankine cycle. *Renew Sustain Energy Rev* 2013;24:325–42. <https://doi.org/10.1016/j.rser.2013.03.040>.
- Quoilin S, Van Den Broek M, Declaye S, Dewalle P, Lemort V. Techno-economic survey of Organic Rankine Cycle (ORC) systems. *Renew Sustain Energy Rev* 2013;22:168–86. <https://doi.org/10.1016/j.rser.2013.01.028>.
- Lecompte S, Huisseune H, Van Den Broek M, Vanslambrouck B, De Paepe M. Review of organic Rankine cycle (ORC) architectures for waste heat recovery. *Renew Sustain Energy Rev* 2015;47:448–61. <https://doi.org/10.1016/j.rser.2015.03.089>.
- Vélez F, Segovia JJ, Martín MC, Antolín G, Chejne F, Quijano A. A technical, economical and market review of organic Rankine cycles for the conversion of low-grade heat for power generation. *Renew Sustain Energy Rev* 2012;16(6):4175–89. <https://doi.org/10.1016/j.rser.2012.03.022>.
- Markides CN. The role of pumped and waste heat technologies in a high-efficiency sustainable energy future for the UK. *Appl Therm Eng* 2013;53(2):197–209. <https://doi.org/10.1016/j.applthermaleng.2012.02.037>.
- Markides CN. Low-concentration solar-power systems based on organic Rankine cycles for distributed-scale applications: overview and further developments. *Front Energy Res* 2015;3:1–16. <https://doi.org/10.3389/feng.2015.00047>. Article number: 47.
- Environmental Investigation Agency (EIA). Kigali amendment to the Montreal protocol: a crucial step in the fight against catastrophic climate change. 2016.
- Freeman J, Hellgardt K, Markides CN. Working fluid selection and electrical performance optimisation of a domestic solar-ORC combined heat and power system for year-round operation in the UK. *Appl Energy* 2017;186:291–303. <https://doi.org/10.1016/j.apenergy.2016.04.041>.
- Oyewunmi OA, Lecompte S, De Paepe M, Markides CN. Thermoeconomic analysis of recuperative sub- and transcritical organic Rankine cycle systems. *Energy Procedia* 2017;129:58–65. <https://doi.org/10.1016/j.egypro.2017.09.187>.
- Drescher U, Brüggemann D. Fluid selection for the organic Rankine cycle (ORC) in biomass power and heat plants. *Appl Therm Eng* 2007;27(1):223–8. <https://doi.org/10.1016/j.applthermaleng.2006.04.024>.
- Schwöbel JAH, Preißinger M, Brüggemann D, Klamt A. High-throughput screening of working fluids for the organic Rankine cycle (ORC) based on conductor-like screening model for realistic solvation (COSMO-RS) and thermodynamic process simulations. *Ind Eng Chem Res* 2017;56:788–98. <https://doi.org/10.1021/acs.iecr.6b03857>.
- Preißinger M, Schwöbel JAH, Klamt A, Brüggemann D. Multi-criteria evaluation of several million working fluids for waste heat recovery by means of organic Rankine cycle in passenger cars and heavy-duty trucks. *Appl Energy* 2017;206:887–99. <https://doi.org/10.1016/j.apenergy.2017.08.212>.
- Vivian J, Manente G, Lazzaretto A. A general framework to select working fluid and configuration of ORCs for low-to-medium temperature heat sources. *Appl Energy* 2015;156:727–46. <https://doi.org/10.1016/j.apenergy.2015.07.005>.
- Lukowski MZ, DiPippo R, Tester JW. Molecular property methods for assessing efficiency of organic Rankine cycles. *Energy* 2018;142:108–20. <https://doi.org/10.1016/j.energy.2017.09.140>.
- Papadopoulos AI, Stijepovic M, Linke P. On the systematic design and selection of optimal working fluids for organic Rankine cycles. *Appl Therm Eng* 2010;30(6–7):760–9.
- Papadopoulos AI, Stijepovic M, Linke P, Seferlis P, Voutetakis S. Toward optimum working fluid mixtures for organic Rankine cycles using molecular design and sensitivity analysis. *Ind Eng Chem Res* 2013;52:12116–33.
- Brignoli R, Brown JS. Organic Rankine cycle model for well-described and not-so-well-described working fluids. *Energy* 2015;86:93–104. <https://doi.org/10.1016/j.energy.2015.03.119>.
- Palma-Flores O, Flores-Tlacuahuac A, Canseco-Melchor G. Simultaneous molecular and process design for waste heat recovery. *Energy* 2016;99:32–47. <https://doi.org/10.1016/j.energy.2016.01.024>.
- Su W, Zhao L, Deng S. Developing a performance evaluation model of organic Rankine cycle for working fluids based on the group contribution method. *Energy Convers Manag* 2017;132:307–15. <https://doi.org/10.1016/j.enconman.2016.11.040>.
- Su W, Zhao L, Deng S. Simultaneous working fluids design and cycle optimization for organic Rankine cycle using group contribution model. *Appl Energy* 2017;202:618–27. <https://doi.org/10.1016/j.apenergy.2017.03.133>.
- Cignitti S, Andreasen JG, Haglind F, Woodley JM, Abildskov J. Integrated working fluid-thermodynamic cycle design of organic Rankine cycle power systems for waste heat recovery. *Appl Energy* 2017;203:442–53. <https://doi.org/10.1016/j.apenergy.2017.06.031>.
- Joback KG, Reid RC. Estimation of pure-component properties from group-contributions. *Chem Eng Commun* 1987;57(1–6):233–43. <https://doi.org/10.1080/00986448708960487>.
- Chapman WG, Gubbins KE, Jackson G, Radosz M. SAFT: equation-of-state solution model for associating fluids. *Fluid Phase Equil* 1989;52(C):31–8. [https://doi.org/10.1016/0378-3812\(89\)80308-5](https://doi.org/10.1016/0378-3812(89)80308-5).

- [33] Chapman WG, Gubbins KE, Jackson G, Radosd M. New reference equation of state for associating liquids. *Ind Eng Chem Res* 1990;29(8):1709–21.
- [34] Lampe M, Stavrou M, Bu HM, Gross J, Bardow A. Simultaneous optimization of working fluid and process for organic Rankine cycles using PC-SAFT. *Ind Eng Chem Res* 2014;53:8821–30.
- [35] Lampe M, Stavrou M, Schilling J, Sauer E, Gross J, Bardow A. Computer-aided molecular design in the continuous-molecular targeting framework using group-contribution PC-SAFT. *Comput Chem Eng* 2015;81:278–87. <https://doi.org/10.1016/j.compchemeng.2015.04.008>.
- [36] Gross J, Sadowski G. Perturbed-chain SAFT: an equation of state based on a perturbation theory for chain molecules. *Ind Eng Chem Res* 2001;40(4):1244–60. <https://doi.org/10.1021/ie0003887>.
- [37] Gross J, Sadowski G. Modeling polymer systems using the perturbed-chain statistical associating fluid theory equation of state. *Ind Eng Chem Res* 2002;41:1084–93. <https://doi.org/10.1021/ie010449g>.
- [38] Schilling J, Lampe M, Bardow A. 1-stage CoMT-CAMD: An approach for integrated design of ORC process and working fluid using PC-SAFT. *Chem Eng Sci* 2017; 217–239. <https://doi.org/10.1016/j.ces.2016.04.048>;159.
- [39] Schilling J, Tillmanns D, Lampe M, Hopp M, Gross J, Bardow A. Integrating working fluid design into the thermo-economic design of ORC processes using PC-SAFT. *Energy Procedia* 2017;129:121–8.
- [40] Quoilin S, Declaye S, Tchanche BF, Lemort V. Thermo-economic optimization of waste heat recovery organic Rankine cycles. *Appl Therm Eng* 2011;31(14–15):2885–93.
- [41] Lecompte S, Huisseune H, van den Broek M, De Schampheleire S, De Paepe M. Part load based thermo-economic optimization of the organic Rankine cycle (ORC) applied to a combined heat and power (CHP) system. *Appl Energy* 2013;111:871–81. <https://doi.org/10.1016/j.apenergy.2013.06.043>.
- [42] Oyewunmi OA, Markides CN. Thermo-economic and heat transfer optimization of working-fluid mixtures in a low-temperature organic Rankine cycle system. *Energies* 2016;9(6):448. <https://doi.org/10.3390/en9060448>.
- [43] Andreasen J, Kaern M, Pierobon L, Larsen U, Haglund F. Multi-objective optimization of organic Rankine cycle power plants using pure and mixed working fluids. *Energies* 2016;9(5):322. <https://doi.org/10.3390/en9050322>.
- [44] Feng Y, Hung TC, Zhang Y, Li B, Yang J, Shi Y. Performance comparison of low-grade ORCs (organic Rankine cycles) using R245fa, pentane and their mixtures based on the thermoeconomic multi-objective optimization and decision makings. *Energy* 2015;93(2015):2018–29. <https://doi.org/10.1016/j.energy.2015.10.065>.
- [45] Angelino G, Colonna Di Paliano P. Multicomponent working fluids for organic Rankine cycles (ORCs). *Energy* 1998;23(6):449–63. [https://doi.org/10.1016/S0360-5442\(98\)00009-7](https://doi.org/10.1016/S0360-5442(98)00009-7).
- [46] Lecompte S, Ameel B, Ziviani D, Van Den Broek M, De Paepe M. Exergy analysis of zeotropic mixtures as working fluids in organic Rankine cycles. *Energy Convers Manag* 2014;85:727–39. <https://doi.org/10.1016/j.enconman.2014.02.028>.
- [47] Fischer J. Comparison of trilateral cycles and organic Rankine cycles. *Energy* 2011;36(10):6208–19. <https://doi.org/10.1016/j.energy.2011.07.041>.
- [48] Smith IK, Stosic N, Mujic E, Kovacevic A. Steam as the working fluid for power recovery from exhaust gases by means of screw expanders. *P I Mech Eng E-J Pro* 2011;225(2):117–25. <https://doi.org/10.1177/2041300910393429>.
- [49] White MT, Oyewunmi OA, Haslam AJ, Markides CN. Industrial waste-heat recovery through integrated computer-aided working-fluid and ORC system optimisation using SAFT- γ Mie. *Energy Convers Manag* 2017;150:851–69. <https://doi.org/10.1016/j.enconman.2017.03.048>.
- [50] Lemmon EW, Huber ML, McLinden MO. NIST standard reference database 23: reference fluid thermodynamic and transport properties-REFPROP. 2013.
- [51] Papaioannou V, Lafitte T, Avendaño C, Adjiman CS, Jackson G, Müller EA, Galindo A. Group contribution methodology based on the statistical associating fluid theory for heteronuclear molecules formed from Mie segments. *J Chem Phys* 2014;140, 054107. <https://doi.org/10.1063/1.4851455>.
- [52] Dufal S, Papaioannou V, Sadeqzadeh M, Pogiatis T, Chremos A, Adjiman CS, Jackson G, Galindo A. Prediction of thermodynamic properties and phase behavior of fluids and mixtures with the SAFT- γ mie group-contribution equation of state. *J Chem Eng Data* 2014;59(10):3272–88. <https://doi.org/10.1021/je500248h>.
- [53] Sastri S, Rao K. A simple method to predict surface tension of organic liquids. *Chem Eng J Biochem Eng J* 1995;59(2):181–6. [https://doi.org/10.1016/0923-0467\(94\)02946-6](https://doi.org/10.1016/0923-0467(94)02946-6).
- [54] Reichenberg D. The viscosity of organic vapors at low pressures. *DSC Rep* 1971;11:484.
- [55] Reichenberg D. The estimation of the viscosities of gases and gas mixtures. In: *Symposium on transport properties of fluids and fluid mixtures, their measurement, estimation, correlation and use*. Glasgow, Scotland: East Kilbride; 1979.
- [56] Sastri S, Rao K. A new group contribution method for predicting viscosity of organic liquids. *Chem Eng J* 1992;50(1):9–25. [https://doi.org/10.1016/0300-9467\(92\)80002-R](https://doi.org/10.1016/0300-9467(92)80002-R).
- [57] Sastri S, Rao K. Quick estimating for thermal conductivity. *Chem Eng* 1993;100(8):106.
- [58] Chung TH, Lee LL, Starling KE. Applications of kinetic gas theories and multiparameter correlation for prediction of dilute gas viscosity and thermal conductivity. *Ind Eng Chem Fundam* 1984;23(1):8–13. <https://doi.org/10.1021/i100013a002>.
- [59] Chung TH, Ailan M, Lee LL, Starling KE. Generalized multiparameter correlation for nonpolar and polar fluid transport properties. *Ind Eng Chem Res* 1988;27(4):671–9. <https://doi.org/10.1021/ie00076a024>.
- [60] Hewitt GF, Shires GL, Bott TR. *Process heat transfer*. CRC Press; 1994.
- [61] Bergman TL, Lavine AS, Incropera FP, DeWitt DP. *Fundamentals of heat and mass transfer*. John Wiley & Sons; 2011.
- [62] Verein Deutscher Ingenieure, VDI heat Atlas. second ed. Springer; 2010.
- [63] Dobson MK, Wattelet JP, Chato JC. Optimal sizing of two-phase heat exchangers. *Tech. rep.* 1993.
- [64] Shah M. A general correlation for heat transfer during film condensation inside pipes. *Int J Heat Mass Tran* 1979;22(4):547–56.
- [65] Chatzopoulou MA, Markides CN. Advancements in organic Rankine cycle system optimisation for combined heat and power applications: components sizing and thermoeconomic considerations. In: *30th International Conference on Efficiency, Cost, Optimization, Simulation and Environmental Impact of Energy Systems*, 2–6th July, San Diego, California, USA; 2017.
- [66] Lemmens S. Cost engineering techniques & their applicability for cost estimation of organic Rankine cycle systems. *Energies* 2016;9(7). <https://doi.org/10.3390/en9070485>.
- [67] Chatzopoulou MA, Markides CN. Thermodynamic optimisation of a high-electrical efficiency integrated internal combustion engine–organic Rankine cycle combined heat and power system. *Appl Energy* 2018;226:1229–51. <https://doi.org/10.1016/j.apenergy.2018.06.022>.
- [68] Seider W, Seader J, Lewin D. *Product and process design principles - synthesis, analysis, and evaluation*. second ed. Hoboken, New Jersey: John Wiley & Sons, Inc.; 2009.
- [69] Turton R, Baile RC, Whiting WB, Shaelwitz JA. *Analysis, synthesis and design of chemical processes*. third ed., vol. 53. Boston, MA 02116: Pearson Education, Inc.; 2009.
- [70] Process Systems Enterprise Ltd. gPROMS. 2017. <http://www.psenterprise.com>.
- [71] Lafitte T, Apostolou A, Avendaño C, Galindo A, Adjiman CS, Müller EA, Jackson G. Accurate statistical associating fluid theory for chain molecules formed from Mie segments. *J Chem Phys* 2013;139(15). <https://doi.org/10.1063/1.4819786>.
- [72] Oyewunmi OA, Taleb AI, Haslam AJ, Markides CN. An assessment of working-fluid mixtures using SAFT-VR Mie for use in organic Rankine cycle systems for waste-heat recovery. *Comput Therm Sci* 2014;6(4):301–16. <https://doi.org/10.1615/2014011116>.
- [73] Oyewunmi OA, Taleb AI, Haslam AJ, Markides CN. On the use of SAFT-VR Mie for assessing large-glide fluorocarbon working-fluid mixtures in organic Rankine cycles. *Appl Energy* 2016;163:263–82. <https://doi.org/10.1016/j.apenergy.2015.10.040>.
- [74] Papaioannou V, Calado F, Lafitte T, Dufal S, Sadeqzadeh M, Jackson G, Adjiman CS, Galindo A. Application of the SAFT- γ Mie group contribution equation of state to fluids of relevance to the oil and gas industry. *Fluid Phase Equil* 2015;416:104–19. <https://doi.org/10.1016/j.fluid.2015.12.041>.
- [75] Freeman J, Hellgardt K, Markides CN. An assessment of solar-powered organic Rankine cycle systems for combined heating and power in UK domestic applications. *Appl Energy* 2015;138:605–20. <https://doi.org/10.1016/j.apenergy.2014.10.035>.
- [76] Freeman J, Guarracino I, Kalogirou SA, Markides CN. A small-scale solar organic Rankine cycle combined heat and power system with integrated thermal energy storage. *Appl Therm Eng* 2017;127:1543–54. <https://doi.org/10.1016/j.applthermaleng.2017.07.163>.
- [77] <http://energnet.net/technology/variable-phase-turbine.html>. Accessed 1 June 2018.
- [78] <https://electratherm.com>. Accessed 1 June 2018.
- [79] Oyewunmi OA, Ferre-Serres S, Lecompte S, van den Broek M, De Paepe M, Markides CN. An assessment of subcritical and trans-critical organic Rankine cycles for waste-heat recovery. *Energy Procedia* 2017;105:1870–6. <https://doi.org/10.1016/j.egypro.2017.03.548>.
- [80] Oyewunmi OA, Kirmse CJW, Pantaleo AM, Markides CN. Performance of working-fluid mixtures in ORC-CHP systems for different heat-demand segments and heat-recovery temperature levels. *Energy Convers Manag* 2017;148:1508–24. <https://doi.org/10.1016/j.enconman.2017.05.078>.
- [81] Pantaleo AM, Fordham J, Oyewunmi OA, De Palma P, Markides CN. Integrating cogeneration and intermittent waste-heat recovery in food processing: microturbines vs. ORC systems in the coffee roasting industry. *Appl Energy* 2018;225:782–96. <https://doi.org/10.1016/j.apenergy.2018.04.097>.
- [82] Lecompte S, Oyewunmi OA, Markides CN, Lazova M, Kaya A, van den Broek M, De Paepe M. Case study of an organic Rankine cycle (ORC) for waste heat recovery from an electric arc furnace (EAF). *Energies* 2017;10(5):649. <https://doi.org/10.3390/en10050649>.
- [83] Pantaleo AM, Camporeale SM, Miliozzi A, Russo V, Shah N, Markides CN. Novel hybrid csp-biomass chp for flexible generation: thermo-economic analysis and profitability assessment. *Appl Energy* 2017;204:994–1006. <https://doi.org/10.1016/j.apenergy.2017.05.019>.
- [84] Camporeale SM, Pantaleo AM, Ciliberti PD, Fortunato B. Cycle configuration analysis and techno-economic sensitivity of biomass external fired gas turbine with bottoming ORC. *Energy Convers Manag* 2015;105:1239–50. <https://doi.org/10.1016/j.enconman.2015.08.069>.
- [85] Camporeale SM, Fortunato B, Torresi M, Turi F, Patanleo AM, Pellerano A. Part

load performance and operating strategies of a natural gas–biomass dual fuelled microturbine for combined heat and power generation. *J Eng Gas Turbines Power* 2015;137(12), 121401. <https://doi.org/10.1115/1.4030499>.

Nomenclature

Abbreviations

CAMD: Computer-aided molecular design
 ORC: Organic Rankine cycle
 SAFT: Statistical associating fluid theory
 SIC: Specific investment cost, £/W

Greek Symbols

ε_r : Recuperator effectiveness
 η : Isentropic efficiency
 μ : Dynamic viscosity, Pa s
 ρ : Density, kg/m³

Roman Symbols

ΔT_{log} : Counter-flow log-mean temperature difference, K
 ΔT_{sh} : Degree of superheating, K
 \dot{m} : Mass flow rate, kg/s
 \dot{Q} : Heat transfer rate, W
 W : Power, W
 PP : Pinch point, K
 Re : Reynolds number
 A : Heat-transfer area, m²
 C_p^0 : Component cost, £

C_n : Number of carbon atoms
 c_p : Specific heat capacity at constant pressure, J/(kg K)
 D : Diameter, m
 F : Material factor
 f : Friction factor
 h : Specific enthalpy, J/kg
 k : Thermal conductivity, W/(m K)
 L : Length, m
 p : Pressure, Pa
 p_r : Reduced pressure
 s : Specific entropy, J/(kg K)
 T : Temperature, K
 U : Overall heat-transfer coefficient, W/(m² K)
 u : Velocity, m/s
 x : Mass fraction of one fluid in a two-fluid mixture
 Z : Cost coefficient
 z : Expander inlet design parameter

Subscripts

1–4: ORC state points
 c : Heat sink/condenser
 co : Condensation
 cr : Critical point
 ds : Desuperheating
 e : Expander
 ev : Evaporation
 h : Heat source/evaporator
 n : Net
 o : Working fluid
 p : Pump
 ph : Preheating
 sh : Superheating